

# Recovery of Future Data via Convolution Nuclear Norm Minimization

Guangcan Liu, *Senior Member, IEEE*, Wayne Zhang



**Abstract**—This paper is about recovering the unseen future data from a given sequence of historical samples, so called as *future data recovery*—a significant problem closely related to time series forecasting. For the first time, we study the problem from a perspective of tensor completion. Namely, we convert future data recovery into a more inclusive problem called *sequential tensor completion* (STC), which is to recover a tensor of *sequential* structure from some entries sampled *arbitrarily* from the tensor. Unlike the *ordinary tensor completion* (OTC) problem studied in the majority of literature, STC has a distinctive setup that the target tensor is *sequential* and *not permutable*, which means that the tensor owns rich spatio-temporal structures. This enables the possibility of restoring the arbitrarily selected missing entries, which is not possible under the framework of OTC. Then we propose two methods to address STC, including Discrete Fourier Transform based  $\ell_1$  minimization ( $\text{DFT}_{\ell_1}$ ) and Convolution Nuclear Norm Minimization (CNNM), where  $\text{DFT}_{\ell_1}$  is indeed a special case of CNNM. Whenever the target tensor is low-rank in some convolution domain, CNNM provably succeeds in solving STC. This immediately gives that  $\text{DFT}_{\ell_1}$  is also successful when the Fourier transform of the target tensor is sparse, as convolution low-rankness is a generalization of Fourier sparsity. Experiments on univariate time series, images and videos show encouraging results.

**Index Terms**—data forecasting, sequential tensor, matrix completion, Fourier transform, convolution, low-rankness, sparsity.

## 1 INTRODUCTION

In many circumstances it is desirable to predict what would happen in future, e.g., the safety of a self-driving vehicle has to account on the prediction of the moving of other vehicles and pedestrians. However, it is theoretically impossible to observe directly the things coming ahead of time. Given this pressing situation, it is crucial to develop computational methods that can recover the future data from historical samples (i.e., data forecasting). Since the data samples can often be organized in tensor form, we would like to formulate mathematically the forecasting problem as follows:

**Problem 1.1** (Future Data Recovery). *Let  $p$  and  $q$  be two pre-specified positive integers. Suppose that  $\{M_t\}_{t=1}^{p+q}$  is a sequence of  $p + q$  order- $(n - 1)$  tensors with  $n \geq 1$ , i.e.,*

*$M_t \in \mathbb{R}^{m_1 \times \cdots \times m_{n-1}}, \forall t \geq 1$ . Given  $\{M_t\}_{t=1}^p$ , can we **identify** the values of  $\{M_t\}_{t=p+1}^{p+q}$ ?*

The above problem is essentially a promotion of *time series forecasting* [1–3], highlighting the identifiability issue as well as the action of generalizing univariate or multivariate sequences to tensor-valued ones, in which each value  $M_t$  itself is a structured tensor. In general, Problem 1.1 has an immense scope that covers a wide range of forecasting problems. For example, when  $n = 1$ ,  $M_t$  is a real number and thus Problem 1.1 falls back to univariate time series forecasting [4]. In the case of  $n = 3$ ,  $M_t$  is of matrix-valued, thereby Problem 1.1 embodies the challenging task of video prediction [5], which aims at obtaining the next  $q$  image frames of a given sequence of  $p$  frames.

A great many approaches for time series analysis have been proposed in the literature, see the surveys in [2, 3]. Classical methods, e.g., Auto-Regressive Moving Average (ARMA) [1] and its extensions, often preset specific models to characterize the evolution of one or multiple variables through time. This type of methods may rely heavily on their parametric settings, and exhaustive model selection is usually necessary for them to attain satisfactory results on fresh datasets. Now it is prevalent to adopt the idea of *data driven*, which suggests utilizing a huge mass of historical sequences to train luxurious models such that the evolution law may emerge autonomously. Such a seemingly “untalented” idea is indeed useful, leading to dozens of promising methods for forecasting [6]. In particular, the methods based on Recurrent Neural Network (RNN) and Long Short-Term Memory (LSTM) [7] have shown superior performance on many datasets, e.g., [8–10]. While impressive, existing studies still have some limitations:

- For the current deep architectures (e.g., [8–10]) to solve Problem 1.1, the most critical hypothesis is that the desired evolution law can be learnt by using sufficient historical sequences to train an over-parameterized network. To obey the hypothesis, one essentially needs to gather a great many training sequences that are similar to  $\{M_t\}_{t=1}^{p+q}$  in structure. This, however, is not always viable in reality, because finding extra data similar to  $\{M_t\}_{t=1}^{p+q}$  is a challenging problem by itself. In that sense, the traditional scheme of working with *only one sequence* is still of considerable significance, and thus we shall focus on the setup of *no extra data* in this paper.

- G. Liu is with B-DAT and CICAET, School of Automation, Nanjing University of Information Science and Technology, Nanjing, China 210044. Email: gcliu@nuist.edu.cn.
- W. Zhang is with SenseTime Research, Harbour View 1 Podium, 12 Science Park East Ave, Hong Kong Science Park, Shatin, N.T., Hong Kong 999077. Email: wayne.zhang@sensetime.com.

- In many applications such as meteorology, the given data  $\{M_t\}_{t=1}^p$  itself may contain missing entries. It is generally challenging for most forecasting methods to cope with such situations [11, 12].
- To our knowledge, there is still a lack of theories that figure out the conditions under which the desired future data is *identifiable*. Such theories are in fact crucially important because, without any restrictions,  $\{M_t\}_{t=p}^{p+q}$  can be arbitrary and thus unpredictable.

To tackle the above issues, we would suggest a different methodology, namely we convert Problem 1.1 into a more general problem as follows. For a tensor-valued time series  $\{M_t\}_{t=1}^{p+q}$  with  $M_t \in \mathbb{R}^{m_1 \times \dots \times m_{n-1}}$ , we define an order- $n$  tensor  $M \in \mathbb{R}^{m_1 \times \dots \times m_n}$  as

$$[M]_{i_1, \dots, i_n} = [M_{i_n}]_{i_1, \dots, i_{n-1}}, 1 \leq i_j \leq m_j, 1 \leq j \leq n,$$

where  $m_n = p + q$  and  $[\cdot]_{i_1, \dots, i_n}$  is the  $(i_1, \dots, i_n)$ th entry of an order- $n$  tensor. That is,  $M$  is formed by concatenating a sequence of order- $(n-1)$  tensors into an order- $n$  one. Subsequently, we define a sampling set  $\Omega \subset \{1, \dots, m_1\} \times \dots \times \{1, \dots, m_n\}$  as in the following:

$$\Omega = \{(i_1, \dots, i_n) : 1 \leq i_j \leq m_j, \forall 1 \leq j \leq n-1 \text{ and } 1 \leq i_n \leq p\}. \quad (1)$$

That is to say,  $\Omega$  is a set consisting of the locations of the observations in  $\{M_t\}_{t=1}^p$  and  $\Omega^\perp$ , the complement set of  $\Omega$ , stores the locations of the unseen future entries in  $\{M_t\}_{t=p+1}^{p+q}$ . With these notations, we turn to a more inclusive problem named *sequential tensor completion* (STC).<sup>1</sup>

**Problem 1.2** (Sequential Tensor Completion). *Let  $M \in \mathbb{R}^{m_1 \times \dots \times m_n}$  be an order- $n$  data tensor formed from some tensor-valued time series, and let  $L_0 \in \mathbb{R}^{m_1 \times \dots \times m_n}$  be a **sequential** tensor of interest that satisfies some regularity conditions and  $L_0 \approx M$ . Suppose that we are given a subset of the entries in  $M$  and a sampling set  $\Omega \subset \{1, \dots, m_1\} \times \dots \times \{1, \dots, m_n\}$  consisting of the locations of observed entries. The configuration of  $\Omega$  is quite progressive, namely the locations of the missing entries included in  $\Omega^\perp$  are allowed to be distributed **arbitrarily**. Can we restore the target tensor  $L_0$ ? If so, under which conditions?*

In this way, Problem 1.1 is incorporated into the scope of tensor completion, which is to fill in the missing entries of a partially observed tensor. Such a scenario has an immediate advantage; that is, it becomes straightforward to handle the difficult cases where the given data  $\{M_t\}_{t=1}^p$  itself is incomplete. Moreover, we insert intentionally a deviation between  $M$  and  $L_0$  in the consideration of the situations in practice: Very often the data tensor  $M$  may not obey strictly the regularity conditions imposed on the target

tensor  $L_0$ . While appealing, Problem 1.2 cannot be solved by *ordinary tensor completion* (OTC) methods, e.g., [13–20], which treat  $L_0$  as an ordinary tensor of permutable. This is because permutability can be in conflict with identifiability: Whenever the target  $L_0$  is permutable and meanwhile some of its slices are *wholly missing*, it is unrealistic to identify  $L_0$ . In other words, *all the models that are invariant to permutation have no application to STC*. Specifically, OTC methods may fill in the missing entries with zeros when the sampling set  $\Omega$  is configured as in (1). Yet, the STC problem could be addressed by a framework similar to OTC:

$$\min_L \phi(L) + \frac{\lambda}{2} \sum_{(i_1, \dots, i_n) \in \Omega} ([L]_{i_1, \dots, i_n} - [M]_{i_1, \dots, i_n})^2, \quad (2)$$

where  $\phi(\cdot)$  is some regularizer and  $\lambda > 0$  is a parameter. As pointed out by [21], the key for solving the forecasting problem is to devise a proper regularizer that can capture the spatio-temporal structures existing in data. To handle the STC problem, the regularizer  $\phi(\cdot)$  should, at least, be sensitive to permutation.<sup>2</sup> Based on this, it is easy to see that the recent techniques in [22, 23] are inapplicable to STC.

In general, the spatio-temporal structures underlying data are varied, and it is hard to handle all of them by a single model. As an example, we would like to consider natural images, videos or something else similar. For such data, it is well-known that the Fourier coefficients of the data tensor are mostly close to zero [24–32], which motivates us to revisit a classical method termed Discrete Fourier Transform (DFT) based  $\ell_1$  minimization ( $\text{DFT}_{\ell_1}$ ). Given a collection of observations,  $\text{DFT}_{\ell_1}$  seeks a tensor that not only possesses the sparsest Fourier representation but also minimizes a squared loss on the observed entries:

$$\min_L \|\mathcal{F}(L)\|_1 + \frac{\lambda}{2} \sum_{(i_1, \dots, i_n) \in \Omega} ([L]_{i_1, \dots, i_n} - [M]_{i_1, \dots, i_n})^2, \quad (3)$$

where  $\mathcal{F}(\cdot)$  is the DFT operator,  $\|\cdot\|_1$  denotes the  $\ell_1$  norm of a tensor seen as a long vector, and  $\lambda > 0$  is a parameter. It is provable that  $\text{DFT}_{\ell_1}$  strictly succeeds in solving STC, as long as the target tensor we want to recover has a sparse representation in the Fourier domain. When the premise is just approximately true,  $\text{DFT}_{\ell_1}$  still guarantees to produce near recovery to the desired tensor. Remarkably, our analysis explains why  $\text{DFT}_{\ell_1}$  can solve STC: *No matter how the missing entries are placed,  $\text{DFT}_{\ell_1}$  converts STC to an OTC problem that always has a well-posed sampling pattern* (see Section 4.1 and Section 4.2). In addition, the optimization problem in (3) is convex and can be solved by any of the many first-order methods, e.g., Alternating Direction Method of Multipliers (ADMM) [33, 34]. To solve problem (3) for an  $m$ -dimensional tensor with  $m = \prod_{j=1}^n m_j$ , ADMM needs only  $O(m \log m)$  time.

While theoretically effective and computationally efficient,  $\text{DFT}_{\ell_1}$  suffers from a drawback that every directions of the tensor are treated equally. This may lead to undesired artifacts while applying the method onto heterogeneous

1. To understand this paper, it is very important to see the difference between sequential and ordinary tensors. In general, ordinary tensors are **permutable** and can be equivalently transformed by reordering their slices, while sequential tensors contain rich spatio-temporal structures and are therefore not permutable. For example, the ratings from some users to a set of movies form an ordinary matrix, whose property is invariant to the permutation of its columns and rows. In contrast, the matrix that represents a natural image is sequential, because the position of each pixel has certain meaning that is not invariant to permutation. Note that we have no intention to claim that the sequential tensors are superior over the ordinary ones, and actually they have very different scopes.

2. Consider the setup of (1). Suppose that  $L_1$  is an optimal solution to (2). Then we could obtain a different  $L_2$  by interchanging  $L_1$ 's two slices whose locations are within  $p+1 \leq i_n \leq p+q$ . If  $\phi(\cdot)$  is invariant to permutation, then  $L_2$  is also optimal to (2), which means that the model cannot identify  $L_0$ .

data, e.g., images and videos. To achieve better recovery performance, we further propose a novel regularizer called *convolution nuclear norm*; that is, the sum of the *convolution eigenvalues* [35] of a tensor. The derived method, *convolution nuclear norm minimization* (CNNM), performs STC by solving the following convex optimization problem:

$$\min_L \|L\|_{\text{cnn}} + \frac{\lambda}{2} \sum_{(i_1, \dots, i_n) \in \Omega} ([L]_{i_1, \dots, i_n} - [M]_{i_1, \dots, i_n})^2, \quad (4)$$

where  $\|\cdot\|_{\text{cnn}}$  is the convolution nuclear norm of a tensor and  $\lambda > 0$  is a parameter. In general, CNNM is a generalization of  $\text{DFT}_{\ell_1}$  which is indeed equivalent to setting the *kernel* in CNNM to have the same size as the target  $L_0$ . By choosing a proper kernel size according to the structure of data, CNNM can outperform dramatically  $\text{DFT}_{\ell_1}$  in terms of recovery accuracy. Similar to  $\text{DFT}_{\ell_1}$ , CNNM also guarantees to exactly (resp. nearly) recover the target  $L_0$ , as long as  $L_0$  has a representation that is low-rank (resp. approximately low-rank) in some convolution domain. Indeed, the theories for CNNM are generalizations of those for  $\text{DFT}_{\ell_1}$ , and they can explain why it is beneficial to control the kernel size. The optimization problem in (4) is convex and can be solved by ADMM in  $O(mk^2)$  time with  $k \ll m$ . Experiments on univariate time series, images and videos demonstrate superior performance of the proposed methods. To summarize, the contributions of this paper mainly include:

- ◊ We propose a new methodology for investigating the data forecasting problem, namely we cast the recovery of future data into a special tensor completion problem termed STC. Compared to the prevalent idea of data driven, our methodology requires no extra training data and can easily handle the cases where the historical data itself is incomplete.
- ◊ We propose a novel method termed CNNM to tackle the STC problem, and we prove that CNNM is successful whenever the target tensor  $L_0$  is low-rank in some convolution domain.
- ◊ Our analysis implies a new result for  $\text{DFT}_{\ell_1}$ , which shows that  $\text{DFT}_{\ell_1}$  strictly succeeds in solving STC provided that the Fourier transform of the target is sparse. Unlike the previous compressive sensing theories, our result is independent of Restricted Isometry Property (RIP) [36], which cannot be obeyed under the context of tensor completion [13].

The rest of this paper is organized as follows. Section 2 summarizes the mathematical notations used throughout the paper. Section 3 explains the technical insights behind the proposed methods. Section 4 is mainly consist of theoretical analysis. Section 5 shows the mathematical proofs of the proposed theories. Section 6 demonstrates empirical results and Section 7 concludes this paper.

## 2 SUMMARY OF MAIN NOTATIONS

Capital letters are used to represent tensors with order 1 or higher, including vectors, matrices and high-order tensors. For an order- $n$  tensor  $X$ ,  $[X]_{i_1, \dots, i_n}$  is the  $(i_1, \dots, i_n)$ th entry of  $X$ . Two types of tensor norms are used frequently throughout the paper: the Frobenius norm given by

$\|X\|_F = \sqrt{\sum_{i_1, \dots, i_n} |[X]_{i_1, \dots, i_n}|^2}$ , and the  $\ell_1$  norm denoted by  $\|\cdot\|_1$  and given by  $\|X\|_1 = \sum_{i_1, \dots, i_n} |[X]_{i_1, \dots, i_n}|$ , where  $|\cdot|$  denotes the magnitude of a real or complex number. Another two frequently used norms are the *operator norm* and *nuclear norm* [37, 38] of order-2 tensors (i.e., matrices), denoted by  $\|\cdot\|$  and  $\|\cdot\|_*$ , respectively.

Calligraphic letters, such as  $\mathcal{F}$ ,  $\mathcal{P}$  and  $\mathcal{A}$ , are used to denote the linear operators. In particular,  $\mathcal{I}$  denotes the identity operator and  $\mathbf{I}$  is the identity matrix. For a linear operator  $\mathcal{L} : \mathbb{H}_1 \rightarrow \mathbb{H}_2$  between Hilbert spaces, its Hermitian adjoint (or conjugate) is denoted as  $\mathcal{L}^*$  and given by

$$\langle \mathcal{L}(X), Y \rangle_{\mathbb{H}_2} = \langle X, \mathcal{L}^*(Y) \rangle_{\mathbb{H}_1}, \forall X \in \mathbb{H}_1, Y \in \mathbb{H}_2, \quad (5)$$

where  $\langle \cdot, \cdot \rangle_{\mathbb{H}_i}$  is the inner product in the Hilbert space  $\mathbb{H}_i$  ( $i = 1$  or  $2$ ). But the subscript is omitted whenever  $\mathbb{H}_i$  refers to a Euclidian space.

The symbol  $\Omega$  is reserved to denote the sampling set consisting of the locations of observed entries. For  $\Omega \subset \{1, \dots, m_1\} \times \dots \times \{1, \dots, m_n\}$ , its *mask tensor* is denoted by  $\Theta_\Omega$  and given by

$$[\Theta_\Omega]_{i_1, \dots, i_n} = \begin{cases} 1, & \text{if } (i_1, \dots, i_n) \in \Omega, \\ 0, & \text{otherwise.} \end{cases}$$

Denote by  $\mathcal{P}_\Omega$  the orthogonal projection onto  $\Omega$ . Then we have the following:

$$\mathcal{P}_\Omega(X) = \Theta_\Omega \circ X \quad \text{and} \quad \Omega = \text{supp}(\Theta_\Omega), \quad (6)$$

where  $\circ$  denotes the Hadamard product and  $\text{supp}(\cdot)$  is the support set of a tensor.

In most cases, we work with real-valued matrices (i.e., order-2 tensors). For a matrix  $X$ ,  $[X]_{i,:}$  is its  $i$ th row, and  $[X]_{:,j}$  is its  $j$ th column. Let  $\omega = \{j_1, \dots, j_l\}$  be a 1D sampling set. Then  $[X]_{\omega,:}$  denotes the submatrix of  $X$  obtained by selecting the rows with indices  $j_1, \dots, j_l$ , and similarly for  $[X]_{:, \omega}$ . For a 2D sampling set  $\Omega \subset \{1, \dots, m_1\} \times \{1, \dots, m_2\}$ , we imagine it as a sparse matrix and define its “rows”, “columns” and “transpose” in a similar way as for matrices. Namely, the  $i$ th row of  $\Omega$  is denoted by  $\Omega_i$  and given by  $\Omega_i = \{i_2 : (i_1, i_2) \in \Omega, i_1 = i\}$ , the  $j$ th column is defined as  $\Omega^j = \{i_1 : (i_1, i_2) \in \Omega, i_2 = j\}$ , and the transpose is given by  $\Omega^T = \{(i_2, i_1) : (i_1, i_2) \in \Omega\}$ .

Letters  $U$  and  $V$  are reserved for the left and right singular vectors of a real-valued matrix, respectively. The orthogonal projection onto the column space  $U$  is denoted by  $\mathcal{P}_U$  and given by  $\mathcal{P}_U(X) = UU^T X$ , and similarly for the row space  $\mathcal{P}_V(X) = XVV^T$ . The same notation is also used to represent a subspace of matrices, e.g., we say that  $X \in \mathcal{P}_U$  for any matrix  $X$  obeying  $\mathcal{P}_U(X) = X$ .

## 3 $\text{DFT}_{\ell_1}$ AND CNNM

This section introduces the technical details of  $\text{DFT}_{\ell_1}$  and CNNM, as well as some preliminary knowledge helpful for understanding the proposed techniques.

### 3.1 Multi-Directional DFT

Multi-directional DFT, also known as multi-dimensional DFT, is a very important concept in signal processing and compressive sensing. Its definition is widely available in the literature and some public websites. Here, we shall present

a definition that would be easy for engineers to understand. First consider the case of  $n = 1$ , i.e., the DFT of a vector  $X \in \mathbb{R}^m$ . In this particular case,  $\mathcal{F}(X)$  can be simply expressed as

$$\mathcal{F}(X) = U_1 X,$$

with  $U_1 \in \mathbb{C}^{m \times m}$  being a complex-valued, symmetric matrix that satisfies  $U_1^H U_1 = U_1 U_1^H = mI$ , where  $(\cdot)^H$  is the conjugate transpose of a complex-valued matrix. We shall call  $U_1$  as the 1D Fourier transform matrix, whose entries are determined once the dimension  $m$  is given. Actually, one can use the Matlab function “dftmtx” to generate this transform matrix.

Similarly, when  $n = 2$ , the DFT of a matrix  $X \in \mathbb{R}^{m_1 \times m_2}$  is given by

$$\mathcal{F}(X) = U_1 X U_2,$$

where  $U_1 \in \mathbb{C}^{m_1 \times m_1}$  and  $U_2 \in \mathbb{C}^{m_2 \times m_2}$  are the 1D Fourier transform matrices for the columns and rows of  $X$ , respectively. For a general order- $n$  tensor  $X \in \mathbb{R}^{m_1 \times \dots \times m_n}$ , its DFT is given by

$$\mathcal{F}(X) = X \times_1 U_1 \cdots \times_n U_n,$$

where  $U_i \in \mathbb{C}^{m_i \times m_i}$  is the 1D Fourier transform matrix for the  $i$ th direction, and  $\times_j$  ( $1 \leq j \leq n$ ) is the *mode- $j$  product* [39] between tensor and matrix.

### 3.2 Convolution Matrix

The concept of (discrete) convolution, the most fundamental concept in signal processing, plays an important role in this paper. Its definition—though mostly unique—has multiple variants, depending on which *boundary condition* is used. What we consider in this paper is the *circular convolution*, i.e., the convolution equipped with *circulant boundary condition* [40]. Let’s begin with the simple case of  $n = 1$ , i.e., the circular convolution procedure of converting  $X \in \mathbb{R}^m$  and  $K \in \mathbb{R}^k$  ( $k \leq m$ ) into  $X \star K \in \mathbb{R}^m$ :

$$[X \star K]_i = \sum_{s=1}^m [X]_{i-s} [K]_s, i = 1, \dots, m,$$

where  $\star$  denotes the convolution operator, and it is assumed that  $[X]_{i-s} = [X]_{i-s+m}$  for  $i \leq s$ ; this is the so-called circulant boundary condition. Note that we assume  $k \leq m$  throughout this paper, and we call the smaller tensor  $K$  as the *kernel*. In general, the convolution operator is linear and can be converted into matrix multiplication:

$$X \star K = \mathcal{A}_k(X) K, \forall X, K,$$

where  $\mathcal{A}_k(X)$  is the *convolution matrix* [35] of a tensor, and the subscript  $k$  is put to remind the readers that the convolution matrix is always associated with a certain kernel size  $k$ . In the light of circular convolution, the convolution matrix  $\mathcal{A}_k(X)$  of a vector  $X = [x_1, \dots, x_m]^T$  is a truncated circulant matrix of size  $m \times k$ :

$$\mathcal{A}_k(X) = \begin{bmatrix} x_1 & x_m & \cdots & x_{m-k+2} \\ x_2 & x_1 & \cdots & x_{m-k+3} \\ \vdots & \vdots & \ddots & \vdots \\ x_m & x_{m-1} & \cdots & x_{m-k+1} \end{bmatrix}.$$

In other words, the  $j$ th column of  $\mathcal{A}_k(X)$  is exactly  $S^{j-1}(X)$  with  $S$  being a circular shift operator:

$$S(X) = [x_m, x_1, x_2, \dots, x_{m-1}]^T. \quad (7)$$

This shift operator is implemented by the Matlab function “circshift”. In the special case of  $k = m$ , the convolution matrix  $\mathcal{A}_m(X)$  is exactly an  $m \times m$  circulant matrix.

Now we turn to the general case of order- $n$  tensors, with  $n \geq 1$ . Suppose that  $X \in \mathbb{R}^{m_1 \times \dots \times m_n}$  and  $K \in \mathbb{R}^{k_1 \times \dots \times k_n}$  are two real-valued order- $n$  tensors. Again, it is assumed that  $k_j \leq m_j, \forall 1 \leq j \leq n$  and  $K$  is called as the kernel. Then the procedure of circularly convolving  $X$  and  $K$  into  $X \star K \in \mathbb{R}^{m_1 \times \dots \times m_n}$  is given by

$$[X \star K]_{i_1, \dots, i_n} = \sum_{s_1, \dots, s_n} [X]_{i_1-s_1, \dots, i_n-s_n} [K]_{s_1, \dots, s_n}.$$

The above convolution procedure can be also converted into matrix multiplication. Let  $\text{vec}(\cdot)$  be the vectorization of a tensor, then we have

$$\text{vec}(X \star K) = \mathcal{A}_k(X) \text{vec}(K), \forall X, K, \quad (8)$$

where  $\mathcal{A}_k(X)$  is an  $m \times k$  matrix, with  $m = \prod_{j=1}^n m_j$  and  $k = \prod_{j=1}^n k_j$ . To compute the convolution matrix of an order- $n$  tensor, one just needs to replace the one-directional circular shift operator given in (7) with a multi-directional one, so as to stay in step with the structure of high-order tensors. For more details, please refer to Section 5.1.

### 3.3 Connections Between DFT and Convolution

Whenever the kernel  $K$  has the same size as the tensor  $X$ , i.e.,  $k_j = m_j, \forall 1 \leq j \leq n$ , the produced convolution matrix,  $\mathcal{A}_m(X)$ , is diagonalized by DFT. The cases of  $n = 1$  and  $n = 2$  are well-known and have been widely used in the literature, e.g., [41, 42]. In effect, the conclusion holds for any  $n \geq 1$ , as pointed out by [43]. To be more precise, let the DFT of  $X$  be  $\mathcal{F}(X) = X \times_1 U_1 \cdots \times_n U_n$ , and denote  $U = U_1 \otimes \dots \otimes U_n$  with  $\otimes$  being the Kronecker product. Then  $U \mathcal{A}_m(X) U^H$  is a diagonal matrix, namely  $U \mathcal{A}_m(X) U^H = m \Sigma$  with  $\Sigma = \text{diag}(\sigma_1, \dots, \sigma_m)$ . Based on the fact that the first column of  $U$  is a vector of all ones, it is easy to see that

$$\begin{aligned} \text{vec}(\mathcal{F}(X)) &= U \text{vec}(X) = U [\mathcal{A}_m(X)]_{:,1} \\ &= [U \mathcal{A}_m(X)]_{:,1} = [\Sigma U]_{:,1} = [\sigma_1, \dots, \sigma_m]^T. \end{aligned}$$

That is, the eigenvalues of the convolution matrix  $\mathcal{A}_m(X)$  are exactly the Fourier frequencies given by  $\mathcal{F}(X)$ . Hence, for any  $X \in \mathbb{R}^{m_1 \times \dots \times m_n}$ , we have

$$\|\mathcal{F}(X)\|_0 = \text{rank}(\mathcal{A}_m(X)), \quad \|\mathcal{F}(X)\|_1 = \|\mathcal{A}_m(X)\|_*,$$

where  $\|\cdot\|_0$  is the  $\ell_0$  (pseudo) norm, i.e., the number of nonzero entries in a tensor. As a consequence, the  $\text{DFT}_{\ell_1}$  program (3) is equivalent to the following real-valued convex optimization problem:

$$\min_L \|\mathcal{A}_m(L)\|_* + \frac{\lambda}{2} \|\mathcal{P}_\Omega(L - M)\|_F^2, \quad (9)$$

where  $\lambda > 0$  is a parameter. Although real-valued and convex, the above problem is hard to solve in a scalable way. Thus the formulation (9) is used only for the purpose of theoretical analysis. It is worth noting that, in the general cases of  $k_j < m_j$ , the convolution matrix  $\mathcal{A}_k(X)$  is a tall matrix instead of a square one. Such convolution matrices, however, cannot be diagonalized by DFT.

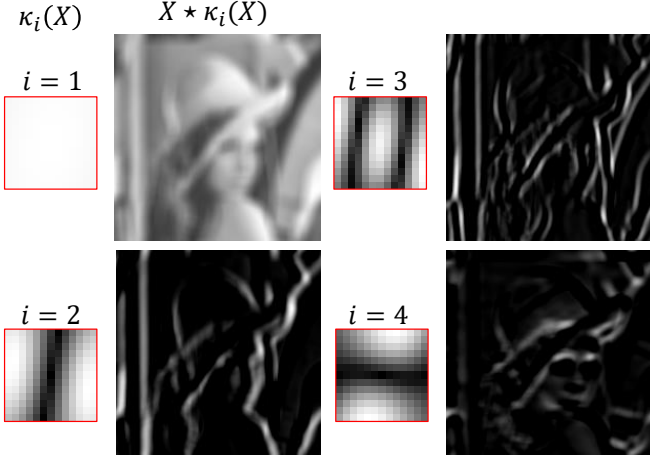


Fig. 1. Visualizing the convolution eigenvectors and filtered signals, using a  $200 \times 200$  Lena image as the experimental data and setting  $k_1 = k_2 = 13$ . For the sake of visual effects, the convolution eigenvector  $\kappa_i(X)$  is processed such that its values are in the range of 0 and 1, and the filtered signal  $X \star \kappa_i(X)$  is normalized to have a maximum of 1.

### 3.4 Convolution Eigenvalues

The concept of convolution eigenvalues is first proposed and investigated by [35], under the context of image deblurring. Although made specific to order-2 tensors (i.e., matrices), the definitions given in [35] can be easily generalized to any order- $n$  tensors.

**Definition 3.1** (Convolution Eigenvalues and Eigenvectors [35]). For a tensor  $X \in \mathbb{R}^{m_1 \times \dots \times m_n}$  associated with a certain kernel size  $k_1 \times \dots \times k_n$  ( $k_j \leq m_j, \forall j$ ), its first convolution eigenvalue is denoted as  $\sigma_1(X)$  and given by

$$\sigma_1(X) = \max_{K \in \mathbb{R}^{k_1 \times \dots \times k_n}} \|X \star K\|_F, \text{ s.t. } \|K\|_F = 1.$$

The maximizer to above problem is called the first convolution eigenvector, denoted as  $\kappa_1(X) \in \mathbb{R}^{k_1 \times \dots \times k_n}$ .

Similarly, the  $i$ th ( $i = 2, \dots, k, k = \prod_{j=1}^n k_j$ ) convolution eigenvalue, denoted as  $\sigma_i(X)$ , is defined by

$$\begin{aligned} \sigma_i(X) &= \max_{K \in \mathbb{R}^{k_1 \times \dots \times k_n}} \|X \star K\|_F, \\ \text{s.t. } &\|K\|_F = 1, \langle K, \kappa_j(X) \rangle = 0, \forall j < i. \end{aligned}$$

The maximizer to above problem is the  $i$ th convolution eigenvector, denoted as  $\kappa_i(X) \in \mathbb{R}^{k_1 \times \dots \times k_n}$ .

Figure 1 shows the first four convolution eigenvectors of a natural image. It can be seen that the convolution eigenvectors are essentially a series of ordered filters, in which the later ones have higher cut-off frequencies. Note that, unlike the traditional singular values of tensors, the convolution eigenvalues of a fixed tensor are not fixed and may vary along with the kernel size.

Due to the relationship given in (8), the convolution eigenvalues are indeed nothing more than the singular values of the convolution matrix, and thus the so-called convolution nuclear norm is exactly the nuclear norm of the convolution matrix:

$$\|X\|_{\text{cnn}} = \|\mathcal{A}_k(X)\|_*, \forall X \in \mathbb{R}^{m_1 \times \dots \times m_n}.$$

Since  $\mathcal{A}_k$  is a linear operator,  $\|X\|_{\text{cnn}}$  is a convex function of  $X$ . As a result, the CNNM program (4) is indeed equivalent to the following real-valued convex program:

$$\min_L \|\mathcal{A}_k(L)\|_* + \frac{\lambda k}{2} \|\mathcal{P}_\Omega(L - M)\|_F^2, \quad (10)$$

where we amplify the parameter  $\lambda$  by a factor of  $k = \prod_{j=1}^n k_j$  for the purpose of normalizing the two objectives to a similar scale. In the extreme case of  $k_j = m_j, \forall j$ , CNNM falls back to  $\text{DFT}_{\ell_1}$ . As aforementioned, it is often desirable to control the kernel size such that  $k \ll m$ . This is actually the primary cause of CNNM's superiority over  $\text{DFT}_{\ell_1}$ .

### 3.5 Optimization Algorithms

**Algorithm for CNNM:** The problem in (10) is convex and can be solved by the standard ADMM algorithm. We first convert (10) to the following equivalent problem:

$$\min_{L, Z} \|Z\|_* + \frac{\lambda k}{2} \|\mathcal{P}_\Omega(L - M)\|_F^2, \text{ s.t. } \mathcal{A}_k(L) = Z.$$

Then the ADMM algorithm minimizes the augmented Lagrangian function,

$$\begin{aligned} &\|Z\|_* + \frac{\lambda k}{2} \|\mathcal{P}_\Omega(L - M)\|_F^2 + \langle \mathcal{A}_k(L) - Z, Y \rangle \\ &+ \frac{\tau}{2} \|\mathcal{A}_k(L) - Z\|_F^2, \end{aligned}$$

with respect to  $L$  and  $Z$ , respectively, by fixing the other variables and then updating the Lagrange multiplier  $Y$  and the penalty parameter  $\tau$ . Namely, while fixing the other variables, the variable  $Z$  is updated by

$$Z = \arg \min_Z \frac{1}{\tau} \|Z\|_* + \frac{1}{2} \|Z - (\mathcal{A}_k(L) + \frac{Y}{\tau})\|_F^2,$$

which is solved via Singular Value Thresholding (SVT) [44]. While fixing the others, the variable  $L$  is updated via

$$L = (\lambda \mathcal{P}_\Omega + \tau \mathcal{I})^{-1} \left( \frac{\mathcal{A}_k^*(\tau Z - Y)}{k} + \lambda \mathcal{P}_\Omega(M) \right),$$

where the inverse operator is indeed simply the entry-wise tensor division. The Lagrange multiplier  $Y$  and penalty parameter  $\tau$  are updated via  $Y = Y + \tau(\mathcal{F}(L) - Z)$  and  $\tau = 1.05\tau$ , respectively. The convergence of ADMM with two or fewer blocks has been well understood, and researchers had even developed advanced techniques to improve its convergence speed, see [33, 45]. While solving our CNNM problem, the computation of each ADMM iteration is dominated by the SVT step, which has a complexity of  $O(mk^2)$ . Usually, the algorithm needs about 200 iterations to get converged.

**Algorithm for  $\text{DFT}_{\ell_1}$ :** The problem in (3) is solved in a similar way to CNNM. The main difference happens in updating the variable  $Z$ , which needs to solve the following convex problem:

$$Z = \arg \min_Z \frac{1}{\tau} \|Z\|_1 + \frac{1}{2} \left\| Z - \left( \mathcal{F}(L) + \frac{Y}{\tau} \right) \right\|_F^2.$$

Note here that the variable  $Z$  is of complex-valued, and thus one needs to invoke Lemma 4.1 of [46] to obtain a closed-form solution; namely,

$$Z = h_{1/\tau} \left( \mathcal{F}(L) + \frac{Y}{\tau} \right),$$

where  $h_\alpha(\cdot)$ , a mapping parameterized by  $\alpha > 0$ , is an entry-wise shrinkage operator given by

$$h_\alpha(z) = \begin{cases} \frac{|z|-\alpha}{|z|}z, & \text{if } |z| > \alpha, \\ 0, & \text{otherwise,} \end{cases} \quad \forall z \in \mathbb{C}. \quad (11)$$

While fixing the others, the variable  $L$  is updated via

$$L = (\lambda \mathcal{P}_\Omega + \tau \mathcal{F}^* \mathcal{F})^{-1} (\mathcal{F}^* (\tau Z - Y) + \lambda \mathcal{P}_\Omega(M)),$$

where  $\mathcal{F}^*$  denotes the Hermitian adjoint of DFT and is indeed given by  $m\mathcal{F}^{-1}$ . Unlike CNM, which needs to perform Singular Value Decomposition (SVD) on tall matrices,  $\text{DFT}_{\ell_1}$  can use the Fast Fourier Transform (FFT) [47] algorithm to compute DFT, and thus has a computational complexity of only  $O(m \log m)$  with  $m = \prod_{j=1}^n m_j$ .

## 4 ANALYSIS

In this section, we will provide theoretical analysis to validate the recovery ability of  $\text{DFT}_{\ell_1}$  and CNM, uncovering the mystery on why our methods can deal with arbitrarily selected missing entries.

### 4.1 Effects of Convolution

According to the conclusions made by most existing studies about tensor completion, it seems “unrealistic” to restore the target  $L_0$  when some of its slices are wholly missing. Consider the case of  $n = 2$ , i.e., matrix completion. It is certain that removing entirely some columns or rows from  $L_0$  will violate the *isomeric condition* [48, 49], which is however necessary for the identifiability of  $L_0$ . Note that, all these assertions are made under the context that  $L_0$  is permutable, which is not the case with STC. As one may have noticed, convolution is indeed a key part of  $\text{DFT}_{\ell_1}$  and CNM, playing a central role in solving the STC problem. In short, the effects of convolution are two-fold: 1) converting a possibly ill-posed sampling pattern to a well-posed one, and 2) reforming the representation of  $L_0$  such that low-rankness may emerge.

**Convolution Sampling Set:** To deal with the sampling set  $\Omega$  with arbitrary, possibly ill-posed pattern, we would introduce a concept called *convolution sampling set*:

**Definition 4.1** (Convolution Sampling Set). For  $\Omega \subset \{1, \dots, m_1\} \times \dots \times \{1, \dots, m_n\}$  with  $m = \prod_{j=1}^n m_j$ , its *convolution sampling set* associated with kernel size  $k_1 \times \dots \times k_n$  is denoted by  $\Omega_A$  and given by

$$\Theta_{\Omega_A} = \mathcal{A}_k(\Theta_\Omega) \quad \text{and} \quad \Omega_A = \text{supp}(\Theta_{\Omega_A}), \quad (12)$$

where  $\Theta_\Omega \in \mathbb{R}^{m_1 \times \dots \times m_n}$  and  $\Theta_{\Omega_A} \in \mathbb{R}^{m \times k}$  are the mask tensor and mask matrix of  $\Omega$  and  $\Omega_A$ , respectively. Note here that the subscript  $k$  is omitted from  $\Omega_A$  for the sake of simplicity.

In general,  $\Omega_A$  is a convolution counterpart of  $\Omega$ , and the corresponding orthogonal projection onto  $\Omega_A$  is given

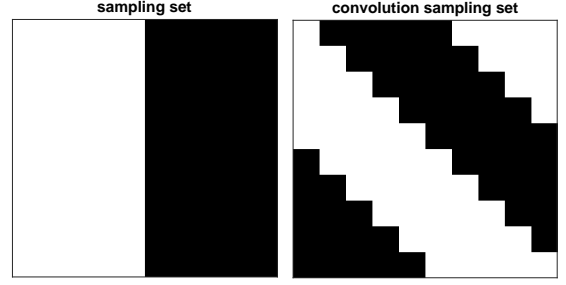


Fig. 2. Illustrating the effects of convolution. Left: the mask matrix  $\Theta_\Omega$  of a sampling set  $\Omega$  with  $m_1 = m_2 = 10$ , where the last 5 columns are wholly missing. Right: the mask matrix  $\Theta_{\Omega_A}$  of the convolution sampling set  $\Omega_A$  with  $k_1 = k_2 = 10$ .

by  $\mathcal{P}_{\Omega_A}(Y) = \Theta_{\Omega_A} \circ Y, \forall Y \in \mathbb{R}^{m \times k}$ . No matter how the missing entries are selected, the convolution sampling set  $\Omega_A$  *always exhibits a well-posed pattern*. Namely, each column of the mask matrix  $\Theta_{\Omega_A}$  has exactly  $\rho_0 m$  ones and  $(1 - \rho_0)m$  zeros, and each row of  $\Theta_{\Omega_A}$  has at most  $(1 - \rho_0)m$  zeros. Whenever  $k_j = m_j, \forall j$ , each row of  $\Theta_{\Omega_A}$  has also exactly  $\rho_0 m$  ones and  $(1 - \rho_0)m$  zeros, as shown in Figure 2.

The following lemma shows some algebraic properties about  $\Omega_A$ , which play an important role in the proofs.

**Lemma 4.1.** Let  $\Omega \subset \{1, \dots, m_1\} \times \dots \times \{1, \dots, m_n\}$ . Suppose that the kernel size used to define  $\mathcal{A}_k$  is given by  $k_1 \times \dots \times k_n$  with  $k_j \leq m_j, \forall 1 \leq j \leq n$ . Denote  $m = \prod_{j=1}^n m_j$  and  $k = \prod_{j=1}^n k_j$ . Let  $\Omega_A \subset \{1, \dots, m\} \times \{1, \dots, k\}$  be the 2D convolution sampling set defined as in (12). For any  $Y \in \mathbb{R}^{m \times k}$  and  $X \in \mathbb{R}^{m_1 \times \dots \times m_n}$ , we have the following:

$$\begin{aligned} \mathcal{A}_k^* \mathcal{A}_k(X) &= kX, \\ \mathcal{A}_k \mathcal{P}_\Omega(X) &= \mathcal{P}_{\Omega_A} \mathcal{A}_k(X), \\ \mathcal{A}_k^* \mathcal{P}_{\Omega_A}(Y) &= \mathcal{P}_\Omega \mathcal{A}_k^*(Y), \end{aligned}$$

where  $\mathcal{A}_k^*$  is the Hermitian adjoint of  $\mathcal{A}_k$ .

**Convolution Rank and Coherence:** In the STC problem, the target tensor  $L_0$  itself is unnecessary to be low-rank. Consider the extreme case of  $n = 1$ , i.e.,  $L_0$  is a vector. In this case,  $L_0$  is always full-rank in the light of Tucker decomposition. Interestingly, such tensors can still have a low *convolution rank*, which is defined as follows. For a tensor  $X \in \mathbb{R}^{m_1 \times \dots \times m_n}$  with kernel size  $k_1 \times \dots \times k_n$ , its *convolution rank* is denoted by  $r_k(X)$  and defined as the number of nonzero convolution eigenvalues, i.e., the rank of its convolution matrix:

$$r_k(X) = \text{rank}(\mathcal{A}_k(X)).$$

It is worth noting that the convolution rank is *not* a generalization of the Tucker rank, as a tensor with low Tucker rank is unnecessarily low-rank in the convolution domain, and vice versa. In some special examples such as the symmetric textures [50], convolution low-rankness and Tucker low-rankness can coexist. But, in general cases, there is no essential connection between these two techniques, and they may have quite different purposes. In short, Tucker rank is oriented to ordinary tensors, while convolution rank is specific to sequential tensors.

To prove that CNM can recover  $L_0$  from a subset of its entries with arbitrary sampling pattern, we need to assume that the convolution rank of  $L_0$  is fairly low. This condition



cannot be met by all kinds of sequential tensors, but there do exist a wide variety of cases of compliable, as we will explain in Section 4.4. Moreover, since  $\mathcal{A}_k(L_0) \in \mathbb{R}^{m \times k}$  is a truncation of  $\mathcal{A}_m(L_0) \in \mathbb{R}^{m \times m}$ , the sparsity degree of the Fourier representation is indeed an upper bound of the convolution rank; namely,

$$r_k(L_0) = \text{rank}(\mathcal{A}_k(L_0)) \leq \text{rank}(\mathcal{A}_m(L_0)) = \|\mathcal{F}(L_0)\|_0.$$

The same as in most existing matrix completion theories, we also need to access the concept of *coherence* [13, 51]. For a tensor  $X \in \mathbb{R}^{m_1 \times \dots \times m_n}$ , suppose that the (skinny) SVD of its convolution matrix is  $\mathcal{A}_k(X) = U\Sigma V^T$ . Then the *convolution coherence* of  $X$  is defined as the coherence of the its convolution matrix  $\mathcal{A}_k(X)$ :

$$\mu_k(X) = \frac{m}{r_k(X)} \max(\max_{1 \leq i \leq m} \|[U]_{i,:}\|_F^2, \max_{1 \leq j \leq m} \|[V]_{j,:}\|_F^2),$$

where  $m = \prod_{j=1}^n m_j$  and  $k = \prod_{j=1}^n k_j$ . As we will show later, the sampling complexity of CNNM—the percentage of observed entries that the method needs in order to restore  $L_0$  successfully—may reply on  $\mu_k(L_0)$ . Candès and Recht [13] had proven that, under certain conditions, the coherence parameters of matrices are bounded from above by some numerical constant.

## 4.2 Dual Problem

By the definition of convolution matrix, recovering  $L_0$  can ensure to recover its convolution matrix  $\mathcal{A}_k(L_0)$ . On the other hand, Lemma 4.1 implies that obtaining  $\mathcal{A}_k(L_0)$  also suffices to recover  $L_0$ . So, STC can be converted into the following *ordinary matrix completion* (OMC) problem:

**Problem 4.1** (Dual Problem). *Use the same notations as in Problem 1.2. Denote by  $\Omega_{\mathcal{A}}$  the convolution sampling set of  $\Omega$ . Assume  $\mathcal{A}_k(L_0) \approx \mathcal{A}_k(M)$ . Given a subset of the entries in  $\mathcal{A}_k(M)$  and the corresponding sampling set  $\Omega_{\mathcal{A}}$ , the goal is to recover the convolution matrix  $\mathcal{A}_k(L_0)$ .*

As aforementioned, the pattern of  $\Omega_{\mathcal{A}}$  is always well-posed, in a sense that some observations are available at every column and row of the matrix.<sup>3</sup> Hence, provided that  $\mathcal{A}_k(L_0)$  is low-rank, Problem 4.1 is exactly the low-rank OMC problem widely studied in the literature [13, 20, 49, 51–54]. However, unlike the setting of random sampling adopted by most studies, the sampling regime here is *deterministic* rather than random, thereby we have to account on the techniques established by [48, 49]. For the completeness of presentation, we would briefly introduce the key techniques followed from [48, 49].

First of all, our analysis needs the concepts of *isomeric condition* (or *isomerism*) and *relative well-conditionedness*.

**Definition 4.2** ( $\Omega/\Omega^T$ -isomeric [48]). *Let  $X \in \mathbb{R}^{m_1 \times m_2}$  be a matrix and  $\Omega \subset \{1, \dots, m_1\} \times \{1, \dots, m_2\}$  be a 2D sampling set. Suppose  $\Omega_i \neq \emptyset$  and  $\Omega^j \neq \emptyset, \forall i, j$ . Then  $X$  is  $\Omega$ -isomeric iff*

$$\text{rank}([X]_{\Omega^j,:}) = \text{rank}(X), \forall j = 1, \dots, m_2.$$

*Furthermore, the matrix  $X$  is called  $\Omega/\Omega^T$ -isomeric iff  $X$  is  $\Omega$ -isomeric and  $X^T$  is  $\Omega^T$ -isomeric.*

3. To meet this, the kernel size needs be chosen properly. For example, under the setup of Problem 1.1,  $k_n$  should be greater than  $q$ .

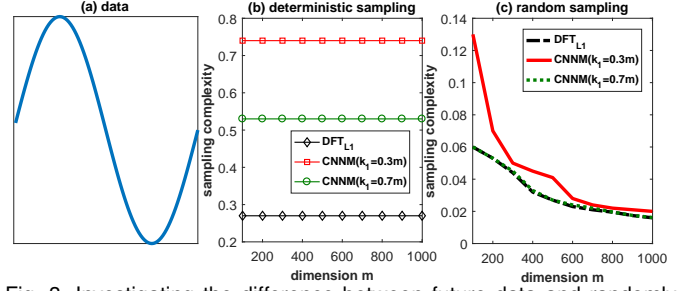


Fig. 3. Investigating the difference between future data and randomly chosen missing entries. (a) The sine sequence used for experiments,  $\{M_t\}_{t=1}^m$  with  $M_t = \sin(2t\pi/m)$ , thereby  $L_0$  is an  $m$ -dimensional vector with  $r_k(L_0) = 2$  and  $\mu_k(L_0) = 1, \forall m \geq k > 2$ . (b) The sampling complexity under the setup of forecasting, where  $\{M_t\}_{t=\rho_0 m+1}^m$  is the missing data. (c) The sampling complexity under the context of random sampling. In these experiments, the complexity is calculated as the smallest fraction of observed entries for the methods to succeed in recovering  $L_0$ , in a sense that the recovery accuracy measured by Peak Signal-to-Noise Ratio (PSNR) is greater than 50.

As pointed out by [49], isomerism is merely a necessary condition for solving OMC, but not sufficient. To compensate the weakness of isomerism, they have proposed an additional condition called *relative well-conditionedness*.

**Definition 4.3** ( $\Omega/\Omega^T$ -relative condition number [49]). *Use the same notations as in Definition 4.2. Suppose that  $[X]_{\Omega^j,:} \neq 0$  and  $[X]_{:, \Omega_i} \neq 0, \forall i, j$ . Then the  $\Omega$ -relative condition number of  $X$  is denoted by  $\gamma_\Omega(X)$  and given by*

$$\gamma_\Omega(X) = \min_{1 \leq j \leq m_2} 1/\|X([X]_{\Omega^j,:})^+\|^2,$$

where  $(\cdot)^+$  is the Moore-Penrose pseudo-inverse of a matrix. Furthermore, the  $\Omega/\Omega^T$ -relative condition number of  $X$  is denoted by  $\gamma_{\Omega, \Omega^T}(X)$  and given by  $\gamma_{\Omega, \Omega^T}(X) = \min(\gamma_\Omega(X), \gamma_{\Omega^T}(X^T))$ .

In order to show that CNNM succeeds in recovering  $L_0$  even when the missing entries are arbitrarily placed, it is necessary to prove that  $\mathcal{A}_k(L_0)$  is  $\Omega_{\mathcal{A}}/\Omega_{\mathcal{A}}^T$ -isomeric and  $\gamma_{\Omega_{\mathcal{A}}, \Omega_{\mathcal{A}}^T}(\mathcal{A}_k(L_0))$  is reasonably large as well. To do this, we need to apply the following lemma.

**Lemma 4.2** ([49]). *Use the same notations as in Definition 4.2, and let  $\Theta_\Omega$  be the mask matrix of  $\Omega$ . Denote by  $\mu_X$  and  $r_X$  the coherence and rank of the matrix  $X$ , respectively. Define a quantity  $\rho$  as*

$$\rho = \min(\min_{1 \leq i \leq m_1} \|\Theta_\Omega[i,:]\|_0/m_2, \min_{1 \leq j \leq m_2} \|\Theta_\Omega[:,j]\|_0/m_1).$$

*For any  $0 \leq \alpha < 1$ , if  $\rho > 1 - (1 - \alpha)/(\mu_X r_X)$  then  $X$  is  $\Omega/\Omega^T$ -isomeric and  $\gamma_{\Omega, \Omega^T}(X) > \alpha$ .*

## 4.3 Main Results

First consider the ideal case where the observed data is precise and noiseless, i.e.,  $\mathcal{P}_\Omega(M - L_0) = 0$ . In this case, as shown below, the target tensor  $L_0$  can be exactly recovered by a simplified version of CNNM (10).

**Theorem 4.1** (Noiseless). *Let  $L_0 \in \mathbb{R}^{m_1 \times \dots \times m_n}$  and  $\Omega \subset \{1, \dots, m_1\} \times \dots \times \{1, \dots, m_n\}$ . Let the adopted kernel size be  $k_1 \times \dots \times k_n$  with  $k_j \leq m_j, \forall 1 \leq j \leq n$ . Denote  $k = \prod_{j=1}^n k_j$ ,  $m = \prod_{j=1}^n m_j$  and  $\rho_0 = \|\Theta_\Omega\|_0/m$ . Denote by  $r_k(L_0)$  and*

$\mu_k(L_0)$  the convolution rank and convolution coherence of the target  $L_0$ , respectively. Assume that  $\mathcal{P}_\Omega(M) = \mathcal{P}_\Omega(L_0)$ . If

$$\rho_0 > 1 - \frac{k}{4\mu_k(L_0)r_k(L_0)m},$$

then the exact solution of  $L = L_0$  is the unique minimizer to the following convex optimization problem:

$$\min_L \|\mathcal{A}_k(L)\|_*, \text{ s.t. } \mathcal{P}_\Omega(L - M) = 0. \quad (13)$$

By setting the kernel to have the same size as the target  $L_0$ , CNNM falls back to  $\text{DFT}_{\ell_1}$ . Thus, the following is indeed an immediate consequence of Theorem 4.1.

**Corollary 4.1** (Noiseless). *Use the same notations as in Theorem 4.1, and set  $k_j = m_j, \forall 1 \leq j \leq n$ . Assume that the observations are noiseless, namely  $\mathcal{P}_\Omega(M) = \mathcal{P}_\Omega(L_0)$ . If*

$$\rho_0 > 1 - \frac{1}{4\mu_m(L_0)\|\mathcal{F}(L_0)\|_0},$$

then the exact solution of  $L = L_0$  is the unique minimizer to the following convex optimization problem:

$$\min_L \|\mathcal{F}(L)\|_1, \text{ s.t. } \mathcal{P}_\Omega(L - M) = 0, \quad (14)$$

which is a simplified version of  $\text{DFT}_{\ell_1}$  (3).

The above theories imply that the sampling complexity, the lower boundary of  $\rho_0$ , has no direct link to the tensor dimension  $m$ . This is quite unlike the random sampling based tensor completion theories (e.g., [13, 55]), which suggest that the sampling complexity for restoring the convolution matrix,  $\mathcal{A}_m(L_0) \in \mathbb{R}^{m \times m}$ , can be as low as  $O(\mu_m(L_0)r_m(L_0)(\log m)^2/m)$  [55], and which gives that the complexity should tend to decrease as  $m$  grows. In fact, there is no conflict because, as pointed out by [49], the sampling regime under forecasting is indeed deterministic rather than random. Figure 3 illustrates that the results derived from random sampling cannot apply to forecasting, confirming the certainty of our result.

Corollary 4.1 implies that Problem 1.1 is solved by the  $\text{DFT}_{\ell_1}$  program (14) provided that  $M = L_0$  and

$$p > q(4\mu_m(L_0)\|\mathcal{F}(L_0)\|_0 - 1).$$

So, in order to succeed in forecasting the future data, it could be helpful to increase the number of historical samples. This will be more clear by looking into the sparsity of  $\mathcal{F}(L_0)$ . For example, when  $\|\mathcal{F}(L_0)\|_0 < m^\beta/\mu_m(L_0)$  with  $0 \leq \beta < 1$ , Corollary 4.1 gives that the next  $q$  values of a given sequence of  $p$  tensors are identified provided that

$$p > 4^{1/(1-\beta)} \tilde{m}^{\beta/(1-\beta)} q^{1/(1-\beta)},$$

where  $\tilde{m} = \prod_{j=1}^{n-1} m_j$  is the dimension of the values in a tensor-valued time series. The interpretation for Theorem 4.1 is similar. The main difference is that CNNM can further reduce the sampling complexity by choosing a proper kernel size, as we will explain in Section 4.4.

The programs in (13) and (14) are designed for the case where the observations are noiseless. This is usually not true in practice and, even more, the convolution matrix of  $M$  is often not strictly low-rank. So, it is more reasonable to consider that there is a deviation between  $M$  and  $L_0$ ; namely,  $\|\mathcal{P}_\Omega(M - L_0)\|_F \leq \epsilon$ . In this case, as we will show

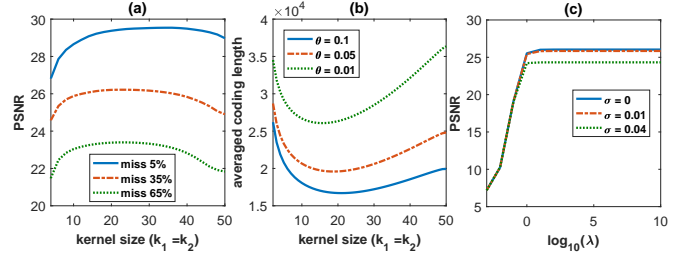


Fig. 4. Exploring the influences of the parameters in CNNM, using a  $50 \times 50$  image patch as the experimental data. (a) Plotting the recovery accuracy as a function of the kernel size. (b) Plotting the averaged coding length as a function of the kernel size. (c) Plotting the recovery accuracy as a function of the parameter  $\lambda$ . For the experiments in (c), the missing rate is set as 35% and the observed entries are contaminated by iid Gaussian noise with mean 0 and standard deviation  $\sigma$ . Note that in this paper the Peak Signal-to-Noise Ratio (PSNR) measure is evaluated only on the missing entries.

soon, the target  $L_0$  can still be accurately recovered by the following program equivalent to (10):

$$\min_L \|\mathcal{A}_k(L)\|_*, \text{ s.t. } \|\mathcal{P}_\Omega(L - M)\|_F \leq \epsilon, \quad (15)$$

where  $\epsilon > 0$  is a parameter.

**Theorem 4.2** (Noisy). *Use the same notations as in Theorem 4.1. Suppose that  $\|\mathcal{P}_\Omega(M - L_0)\|_F \leq \epsilon$ . If*

$$\rho_0 > 1 - \frac{0.22k}{\mu_k(L_0)r_k(L_0)m},$$

then any optimal solution  $L_o$  to the CNNM program (15) gives a near recovery to the target tensor  $L_0$ , in a sense that

$$\|L_o - L_0\|_F \leq (1 + \sqrt{2})(38\sqrt{k} + 2)\epsilon.$$

**Corollary 4.2** (Noisy). *Use the same notations as in Theorem 4.1, and set  $k_j = m_j, \forall j$ . Suppose that  $\|\mathcal{P}_\Omega(M - L_0)\|_F \leq \epsilon$  and  $L_o$  is an optimal solution to the following  $\text{DFT}_{\ell_1}$  program:*

$$\min_L \|\mathcal{F}(L)\|_1, \text{ s.t. } \|\mathcal{P}_\Omega(L - M)\|_F \leq \epsilon. \quad (16)$$

If  $\rho_0 > 1 - 0.22/(\mu_m(L_0)\|\mathcal{F}(L_0)\|_0)$ , then  $L_o$  gives a near recovery to  $L_0$ , in a sense that

$$\|L_o - L_0\|_F \leq (1 + \sqrt{2})(38\sqrt{m} + 2)\epsilon.$$

It is worthy of noting that, interestingly, the results in Theorem 4.2 and Corollary 4.2 are valid even if the data tensor  $M$  does not have any low-rank structures at all. This is because, for any tensor  $M$ , one can always decompose it into  $M = L_0 + N$  with  $\mathcal{A}_k(L_0)$  being strictly low-rank and  $\|N\|_F \leq \epsilon$ . This, however, does not mean that CNNM and  $\text{DFT}_{\ell_1}$  can work well on all datasets: Whenever low-rankness is absent from  $M$ , the residual  $\epsilon$  could be large and the obtained estimate is unnecessarily accurate. For our methods to produce satisfactory results, it is required that the convolution rank of the data tensor  $M$  is low or approximately so.

## 4.4 Discussions

**On Influences of Parameters:** The hyper-parameters in CNNM mainly include the kernel size  $k_1 \times \dots \times k_n$  and the regularization parameter  $\lambda$ . According to the results in Figure 3, it seems beneficial to use large kernels. But this is not the case with most real-world datasets. As shown in



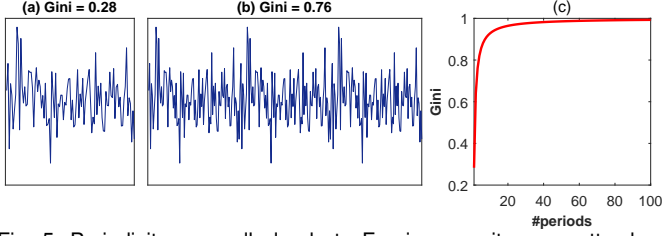


Fig. 5. Periodicity generally leads to Fourier sparsity, no matter how complicate the structure of a single period is. The sparsity degree is measured by Gini index [57], which ranges from 0 to 1. (a) The signal of one period consisting of 50 random numbers. (b) The signal of three periods obtained by repeating the signal in (a) three times. (c) Gini index versus the number of periods.

Figure 4(a), the recovery accuracy of CNNM increases as the enlargement of the adopted kernel size at first, but then drops eventually as the kernel size continues to grow. In fact, both phenomena are consistent with our theories, which imply that the sampling complexity  $\rho_0$  is bounded from below by a quantity dominated by  $r_k(L_0)/k$ . For the particular example in Figure 3,  $r_k(L_0) \equiv 2, \forall k \geq 2$ , and thus large  $k$  produces better recovery. However, in most real-world datasets, the convolution rank may increase as the kernel size grows. To show the consistence in this case, we would like to investigate empirically the *coding length* [56] of the convolution matrix of  $L_0$ :

$$\begin{aligned} \text{CL}_\theta(\mathcal{A}_k(L_0)) \\ = \frac{1}{2}(m+k) \log \det \left( \mathbf{I} + \frac{m}{k\theta^2} \mathcal{A}_k(L_0)(\mathcal{A}_k(L_0))^T \right), \end{aligned}$$

where  $\det(\cdot)$  is the determinant of a matrix and  $\theta > 0$  is a parameter. In general,  $\text{CL}_\theta(\mathcal{A}_k(L_0))$  is no more than a computationally-friendly approximate to  $r_k(L_0)$ , thereby a reasonable approximate to  $r_k(L_0)/k$  is given by

$$\begin{aligned} \text{ACL}_\theta(\mathcal{A}_k(L_0)) &= \frac{\text{CL}_\theta(\mathcal{A}_k(L_0))}{k} \\ &= \frac{1}{2} \left( \frac{m}{k} + 1 \right) \log \det \left( \mathbf{I} + \frac{m}{k\theta^2} \mathcal{A}_k(L_0)(\mathcal{A}_k(L_0))^T \right), \end{aligned}$$

where  $\text{ACL}_\theta(\cdot)$  is the *averaged coding length* of a matrix.

As we can see from Figure 4(b), the averaged coding length of  $\mathcal{A}_k(L_0)$  is minimized at some value between  $k = 1$  and  $k = m$ , and, interestingly, the minimizer can coincide with the point that maximizes the recovery accuracy provided that the parameter  $\theta$  is chosen properly. So, to achieve the best performance, the kernel size in CNNM has to be chosen carefully, which is not easy. Fortunately, CNNM is in fact a reliable method and seldom breaks down unless the kernel is too small (e.g.,  $k_j = 1, \forall j$ ). While applying CNNM to natural images, it is moderately good to use  $k_1 = k_2 = 13$ , as will be shown in our experiments.

Figure 4(c) shows the influence of the parameter  $\lambda$ . It can be seen that there is no loss to enlarge  $\lambda$ . The reason is that we evaluate the recovery accuracy on the missing entries only. So, no matter whether the observations are contaminated by noise or not, we would suggest setting  $\lambda = 1000$  for CNNM and  $\text{DFT}_{\ell_1}$ . To remove the noise possibly existing in the observations, one may use some denoising method to postprocess the results.

**On Fourier Sparsity and Convolution Low-Rankness:** The proposed methods,  $\text{DFT}_{\ell_1}$  and CNNM, depend directly or

indirectly on the sparsity of DFT—the phenomenon that most of the Fourier coefficients of a signal are zero or approximately so, which appears frequently in many domains, ranging from images [26] and videos [24] to Boolean functions [30] and wideband channels [29]. For a 1D signal of  $m$ -dimensional vector, it is well-known that the sparsity will show up whenever a pattern is observed repeatedly over time or, in other words, the signal is periodic (or near periodic) and the series has lasted long enough (i.e.,  $m$  is large), as confirmed by Figure 5. Such an explanation, however, would not generalize to high-order tensors, in which there are multiple time-like directions.

Convolution low-rankness, a generalization of Fourier sparsity, is more interpretable. When  $n = 1$  and  $L_0$  is a vector, the  $j$ th column of the convolution matrix  $\mathcal{A}_k(L_0)$  is simply the vector obtained by circularly shifting the entries in  $L_0$  by  $j - 1$  positions. Now, one may see why or why not  $\mathcal{A}_k(L_0)$  is low-rank. More precisely, when  $L_0$  possesses substantial continuity and the shift degree is relatively small, the signals before and after circular shift are mostly the same and therefore the low-rankness of  $\mathcal{A}_k(L_0)$  will present. Otherwise, the shift operator might cause miss-alignment and prevent low-rankness—but this is not absolute: A non-periodic signal full of dynamics and discontinuities can happen to have a convolution matrix of approximately low-rank (see the lower left part of Figure 7). The general case of order- $n$  tensors is similar, and the only difference is that a multi-directional shift operator is used to move the entries of a tensor along multiple directions.

Beneath it all, the Fourier sparsity and convolution low-rankness are not intuitive phenomena that come out very clearly in their interpretations, and it is hard to determine the exact scope of CNNM and  $\text{DFT}_{\ell_1}$ . Our theories show that, when the degree of convolution low-rankness declines, the performance of CNNM (and  $\text{DFT}_{\ell_1}$ ) is depressed, in the sense that the required sampling complexity has to increase—the forecasting ability will be deprived when the convolution rank exceeds certain threshold. Hence, roughly, our methods are applicable to natural images, videos or something else similar.

**Connections Between  $\text{DFT}_{\ell_1}$  and RNN:** In the light of *learning-based optimization* [58, 59],  $\text{DFT}_{\ell_1}$  is actually related to RNN. Consider the optimization problem in (3). Suppose that the DFT of  $L$  is given by  $\mathcal{F}(L) = L \times_1 U_1 \cdots \times_n U_n$ . Then we have  $\text{vec}(\mathcal{F}(L)) = U \text{vec}(L)$ , where  $U = U_1 \otimes \cdots \otimes U_n$ . Taking  $Y = \text{vec}(L)$ , one can see that the formulation of  $\text{DFT}_{\ell_1}$  is indeed equivalent to

$$\min_{Y \in \mathbb{R}^m} \|UY\|_1 + \frac{\lambda}{2} \|SY - B\|_F^2,$$

where  $B = \text{vec}(\mathcal{P}_\Omega(M)) \in \mathbb{R}^m$  and  $S \in \mathbb{R}^{m \times m}$  is a selection matrix that satisfies  $S \text{vec}(Z) = \text{vec}(\mathcal{P}_\Omega(Z)), \forall Z \in \mathbb{R}^{m_1 \times \cdots \times m_n}$ . Now, taking  $X = UY$  simply leads to

$$\min_{X \in \mathbb{C}^m} \|X\|_1 + \frac{\lambda}{2} \|AX - B\|_F^2,$$

where  $A = SU^H$ . The above problem can be solved by the Iterative Shrinkage and Thresholding Algorithm (ISTA) [60],

which iterates the following procedure:

$$X_{k+1} = h_{1/(\lambda\rho)} \left( X_k - \frac{A^H(AX_k - B)}{\rho} \right),$$

where  $h_\alpha(\cdot)$  is an entry-wise shrinkage operator given by (11). Take  $W = \mathbf{I} - A^H A / \rho = \mathbf{I} - USU^H / \rho$  and  $D = A^H B / \rho = U \text{Svec}(\mathcal{P}_\Omega(M)) / \rho$ . Then we have

$$X_{k+1} = h_{1/(\lambda\rho)}(WX_k + D).$$

So, DFT $_{\ell_1}$  is essentially a particular RNN with activation function  $h_\alpha(\cdot)$ , and the resulted network parameters are fixed complex numbers determined by the Fourier basis.

CNNM is somehow related to the well-known Convolutional Neural Network (CNN) [61]. But the exact relationship is complicate and hard to figure out.

## 5 MATHEMATICAL PROOFS

This section presents in detail the proofs to the proposed lemmas and theorems.

### 5.1 Proof to Lemma 4.1

*Proof.* Denote by  $\mathcal{S}$  the ‘‘circshift’’ operator in Matlab; namely,  $\mathcal{S}(G, u, v)$  circularly shifts the elements in tensor  $G$  by  $u$  positions along the  $v$ th direction. For any  $(i_1, \dots, i_n) \in \{1, \dots, k_1\} \times \dots \times \{1, \dots, k_n\}$ , we define an invertible operator  $\mathcal{T}_{(i_1, \dots, i_n)} : \mathbb{R}^{m_1 \times \dots \times m_n} \rightarrow \mathbb{R}^m$  as

$$\mathcal{T}_{(i_1, \dots, i_n)}(G) = \text{vec}(G_n), \forall G \in \mathbb{R}^{m_1 \times \dots \times m_n},$$

where  $\text{vec}(\cdot)$  is the vectorization operator and  $G_n$  is determined by the following recursive rule:

$$G_0 = G, G_h = \mathcal{S}(G_{h-1}, i_h - 1, h), 1 \leq h \leq n.$$

Suppose that  $j = 1 + \sum_{a=1}^n (i_a - 1) \Pi_{b=0}^{a-1} k_b$ , where it is assumed conveniently that  $k_0 = 1$ . Then we have

$$[\mathcal{A}_k(X)]_{:,j} = \mathcal{T}_{(i_1, \dots, i_n)}(X). \quad (17)$$

According to the definition of the Hermitian adjoint operator given in (5), we have

$$\mathcal{A}_k^*(Z) = \sum_{i_1, \dots, i_n} \mathcal{T}_{(i_1, \dots, i_n)}^{-1}([Z]_{:,j}), \forall Z \in \mathbb{R}^{m \times k}, \quad (18)$$

where it is worth noting that the number  $j$  functionally depends on the index  $(i_1, \dots, i_n)$ . By (17) and (18),

$$\mathcal{A}_k^* \mathcal{A}_k(X) = \sum_{i_1, \dots, i_n} \mathcal{T}_{(i_1, \dots, i_n)}^{-1} \mathcal{T}_{(i_1, \dots, i_n)}(X) = kX.$$

The second claim is easy to prove. By (6), (12) and (17),

$$\begin{aligned} [\mathcal{A}_k \mathcal{P}_\Omega(X)]_{:,j} &= \mathcal{T}_{(i_1, \dots, i_n)}(\Theta_\Omega \circ X) = \\ \mathcal{T}_{(i_1, \dots, i_n)}(\Theta_\Omega) \circ \mathcal{T}_{(i_1, \dots, i_n)}(X) &= [\Theta_{\Omega_A}]_{:,j} \circ [\mathcal{A}_k(X)]_{:,j} \\ &= [\mathcal{P}_{\Omega_A} \mathcal{A}_k(X)]_{:,j}. \end{aligned}$$

It remains to prove the third claim. By (6) and (12),

$$\mathcal{A}_k^* \mathcal{P}_{\Omega_A}(Y) = \mathcal{A}_k^*(\Theta_{\Omega_A} \circ Y) = \mathcal{A}_k^*(\mathcal{A}_k(\Theta_\Omega) \circ Y),$$

which, together with (17) and (18), gives that

$$\begin{aligned} \mathcal{A}_k^* \mathcal{P}_{\Omega_A}(Y) &= \sum_{i_1, \dots, i_n} \mathcal{T}_{(i_1, \dots, i_n)}^{-1}([\mathcal{A}_k(\Theta_\Omega) \circ Y]_{:,j}) \\ &= \sum_{i_1, \dots, i_n} \mathcal{T}_{(i_1, \dots, i_n)}^{-1}([\mathcal{A}_k(\Theta_\Omega)]_{:,j}) \circ \mathcal{T}_{(i_1, \dots, i_n)}^{-1}([Y]_{:,j}) \\ &= \sum_{i_1, \dots, i_n} \Theta_\Omega \circ \mathcal{T}_{(i_1, \dots, i_n)}^{-1}([Y]_{:,j}) = \mathcal{P}_\Omega \mathcal{A}_k^*(Y). \end{aligned}$$

□

### 5.2 Proof to Theorem 4.1

The proof process is quite standard. We shall first prove the following lemma that establishes the conditions under which the solution to (13) is unique and exact.

**Lemma 5.1.** *Suppose the SVD of the convolution matrix of  $L_0$  is given by  $\mathcal{A}_k(L_0) = U_0 \Sigma_0 V_0^T$ . Denote by  $\mathcal{P}_{T_0}(\cdot) = U_0 U_0^T(\cdot) + (\cdot) V_0 V_0^T - U_0 U_0^T(\cdot) V_0 V_0^T$  the orthogonal projection onto the sum of  $U_0$  and  $V_0$ . Then  $L_0$  is the unique minimizer to the problem in (13) provided that:*

1.  $\mathcal{P}_{\Omega_A}^\perp \cap P_{T_0} = \{0\}$ .
2. *There exists  $Y \in \mathbb{R}^{m \times k}$  such that  $P_{T_0} \mathcal{P}_{\Omega_A}(Y) = U_0 V_0^T$  and  $\|P_{T_0}^\perp \mathcal{P}_{\Omega_A}(Y)\| < 1$ .*

*Proof.* Take  $W = P_{T_0}^\perp \mathcal{P}_{\Omega_A}(Y)$ . Then  $\mathcal{A}_k^*(U_0 V_0^T + W) = \mathcal{A}_k^* \mathcal{P}_{\Omega_A}(Y)$ . By Lemma 4.1,

$$\mathcal{A}_k^* \mathcal{P}_{\Omega_A}(Y) = \mathcal{P}_\Omega \mathcal{A}_k^*(Y) \in \mathcal{P}_\Omega.$$

By the standard convexity arguments shown in [62],  $L_0$  is an optimal solution to the convex optimization problem in (13).

It remains to prove that  $L_0$  is the unique minimizer. To do this, we consider a feasible solution  $L_0 + \Delta$  with  $\mathcal{P}_\Omega(\Delta) = 0$ , and we shall show that the objective value strictly increases unless  $\Delta = 0$ . Due to the convexity of nuclear norm, we have

$$\begin{aligned} \|\mathcal{A}_k(L_0 + \Delta)\|_* - \|\mathcal{A}_k(L_0)\|_* &\geq \langle \mathcal{A}_k^*(U_0 V_0^T + H), \Delta \rangle \\ &= \langle U_0 V_0^T + H, \mathcal{A}_k(\Delta) \rangle, \end{aligned}$$

where  $H \in \mathcal{P}_{T_0}^\perp$  and  $\|H\| \leq 1$ . By the duality between the operator and nuclear norms, we can always choose an  $H$  such that

$$\langle H, \mathcal{A}_k(\Delta) \rangle = \|\mathcal{P}_{T_0}^\perp \mathcal{A}_k(\Delta)\|_*.$$

In addition, it follows from Lemma 4.1 that

$$\langle \mathcal{P}_{\Omega_A}(Y), \mathcal{A}_k(\Delta) \rangle = \langle Y, \mathcal{P}_{\Omega_A} \mathcal{A}_k(\Delta) \rangle = \langle Y, \mathcal{A}_k \mathcal{P}_\Omega(\Delta) \rangle = 0.$$

Hence, we have

$$\begin{aligned} \langle U_0 V_0^T + H, \mathcal{A}_k(\Delta) \rangle &= \langle \mathcal{P}_{\Omega_A}(Y) + H - W, \mathcal{A}_k(\Delta) \rangle \\ &= \langle H - W, \mathcal{A}_k(\Delta) \rangle \geq (1 - \|W\|) \|\mathcal{P}_{T_0}^\perp \mathcal{A}_k(\Delta)\|_*. \end{aligned}$$

Since  $\|W\| < 1$ ,  $\|\mathcal{A}_k(L_0 + \Delta)\|_*$  is greater than  $\|\mathcal{A}_k(L_0)\|_*$  unless  $\mathcal{A}_k(\Delta) \in \mathcal{P}_{T_0}$ . Note that  $\mathcal{P}_{\Omega_A} \mathcal{A}_k(\Delta) = \mathcal{A}_k \mathcal{P}_\Omega(\Delta) = 0$ , i.e.,  $\mathcal{A}_k(\Delta) \in \mathcal{P}_{\Omega_A}^\perp$ . Since  $\mathcal{P}_{\Omega_A}^\perp \cap \mathcal{P}_{T_0} = \{0\}$ , it follows that  $\mathcal{A}_k(\Delta) = 0$ , which immediately leads to  $\Delta = 0$ . □

In the rest of the proof, we shall show how we will prove the dual conditions listed in Lemma 5.1. Notice that, even if the locations of the missing entries are arbitrarily distributed, each column of  $\Omega_A$  has exactly a

cardinality of  $\rho_0 m$ , and each row of  $\Omega_{\mathcal{A}}$  contains at least  $k - (1 - \rho_0)m$  elements. Denote by  $\rho$  the smallest sampling complexity of each row and column of  $\Omega_{\mathcal{A}}$ . Provided that  $\rho_0 > 1 - 0.25k/(\mu_k(L_0)r_k(L_0)m)$ , we have

$$\rho \geq \frac{k - (1 - \rho_0)m}{k} > 1 - \frac{0.25}{\mu_k(L_0)r_k(L_0)}.$$

Then it follows from Lemma 4.2 that  $\mathcal{A}_k(L_0)$  is  $\Omega_{\mathcal{A}}/\Omega_{\mathcal{A}}^T$ -isomeric and  $\gamma_{\Omega_{\mathcal{A}}, \Omega_{\mathcal{A}}^T}(\mathcal{A}_k(L_0)) > 0.75$ . Thus, according to Lemma 5.11 of [49], we have

$$\|\mathcal{P}_{T_0} \mathcal{P}_{\Omega_{\mathcal{A}}}^\perp \mathcal{P}_{T_0}\| \leq 2(1 - \gamma_{\Omega_{\mathcal{A}}, \Omega_{\mathcal{A}}^T}(\mathcal{A}_k(L_0))) < 0.5 < 1,$$

which, together with Lemma 5.6 of [49], results in  $\mathcal{P}_{\Omega_{\mathcal{A}}}^\perp \cap \mathcal{P}_{T_0} = \{0\}$ . As a consequence, we could define  $Y$  as

$$Y = \mathcal{P}_{\Omega_{\mathcal{A}}} \mathcal{P}_{T_0} (\mathcal{P}_{T_0} \mathcal{P}_{\Omega_{\mathcal{A}}} \mathcal{P}_{T_0})^{-1} (U_0 V_0^T).$$

It can be verified that  $\mathcal{P}_{T_0} \mathcal{P}_{\Omega_{\mathcal{A}}}(Y) = U_0 V_0^T$ . Moreover, it follows from Lemma 5.12 of [49] that

$$\begin{aligned} \|\mathcal{P}_{T_0}^\perp \mathcal{P}_{\Omega_{\mathcal{A}}}(Y)\| &\leq \|\mathcal{P}_{T_0}^\perp \mathcal{P}_{\Omega_{\mathcal{A}}} \mathcal{P}_{T_0} (\mathcal{P}_{T_0} \mathcal{P}_{\Omega_{\mathcal{A}}} \mathcal{P}_{T_0})^{-1}\| \|U_0 V_0^T\| \\ &= \sqrt{\frac{1}{1 - \|\mathcal{P}_{T_0} \mathcal{P}_{\Omega_{\mathcal{A}}}^\perp \mathcal{P}_{T_0}\|}} - 1 < 1, \end{aligned}$$

which finishes to construct the dual certificate.

### 5.3 Proof to Theorem 4.2

*Proof.* Let  $N = L_o - L_0$  and denote  $N_{\mathcal{A}} = \mathcal{A}_k(N)$ . Notice that  $\|\mathcal{P}_{\Omega}(L_o - M)\|_F \leq \epsilon$  and  $\|\mathcal{P}_{\Omega}(M - L_0)\|_F \leq \epsilon$ . By triangle inequality,  $\|\mathcal{P}_{\Omega}(N)\|_F \leq 2\epsilon$ . Thus,

$$\|\mathcal{P}_{\Omega_{\mathcal{A}}}(N_{\mathcal{A}})\|_F^2 = \|\mathcal{A}_k \mathcal{P}_{\Omega}(N)\|_F^2 = k \|\mathcal{P}_{\Omega}(N)\|_F^2 \leq 4k\epsilon^2.$$

To bound  $\|N\|_F$ , it is sufficient to bound  $\|N_{\mathcal{A}}\|_F$ . So, it remains to bound  $\|\mathcal{P}_{\Omega_{\mathcal{A}}}^\perp(N_{\mathcal{A}})\|_F$ . To do this, we define  $Y$  and  $W$  in the same way as in the proof to Theorem 4.1. Since  $L_o = L_0 + N$  is an optimal solution to (16), we have the following:

$$\begin{aligned} 0 &\geq \|\mathcal{A}_k(L_0 + N)\|_* - \|\mathcal{A}_k(L_0)\|_* \\ &\geq (1 - \|W\|) \|\mathcal{P}_{T_0}^\perp(N_{\mathcal{A}})\|_* + \langle \mathcal{P}_{\Omega_{\mathcal{A}}}(Y), N_{\mathcal{A}} \rangle. \end{aligned}$$

Provided that  $\rho_0 > 1 - 0.22/(\mu(L_0)r(L_0))$ , we can prove that  $\|W\| = \|\mathcal{P}_{T_0}^\perp \mathcal{P}_{\Omega_{\mathcal{A}}}(Y)\| < 0.9$ . As a consequence, we have the following:

$$\begin{aligned} \|\mathcal{P}_{T_0}^\perp(N_{\mathcal{A}})\|_* &\leq -10 \langle \mathcal{P}_{\Omega_{\mathcal{A}}}(Y), \mathcal{P}_{\Omega_{\mathcal{A}}}(N_{\mathcal{A}}) \rangle \\ &\leq 10 \|\mathcal{P}_{\Omega_{\mathcal{A}}}(Y)\| \|\mathcal{P}_{\Omega_{\mathcal{A}}}(N_{\mathcal{A}})\|_* \leq 19 \|\mathcal{P}_{\Omega_{\mathcal{A}}}(N_{\mathcal{A}})\|_* \\ &\leq 19\sqrt{k} \|\mathcal{P}_{\Omega_{\mathcal{A}}}(N_{\mathcal{A}})\|_F \leq 38k\epsilon, \end{aligned}$$

from which it follows that  $\|\mathcal{P}_{T_0}^\perp(N_{\mathcal{A}})\|_F \leq \|\mathcal{P}_{T_0}^\perp(N_{\mathcal{A}})\|_* \leq 38k\epsilon$ , and which simply leads to

$$\|\mathcal{P}_{T_0}^\perp \mathcal{P}_{\Omega_{\mathcal{A}}}^\perp(N_{\mathcal{A}})\|_F \leq (38k + 2\sqrt{k})\epsilon.$$

We also have

$$\begin{aligned} &\|\mathcal{P}_{\Omega_{\mathcal{A}}} \mathcal{P}_{T_0} \mathcal{P}_{\Omega_{\mathcal{A}}}^\perp(N_{\mathcal{A}})\|_F^2 \\ &= \langle \mathcal{P}_{T_0} \mathcal{P}_{\Omega_{\mathcal{A}}} \mathcal{P}_{T_0} \mathcal{P}_{\Omega_{\mathcal{A}}}^\perp(N_{\mathcal{A}}), \mathcal{P}_{T_0} \mathcal{P}_{\Omega_{\mathcal{A}}}^\perp(N_{\mathcal{A}}) \rangle \\ &\geq (1 - \|\mathcal{P}_{T_0} \mathcal{P}_{\Omega_{\mathcal{A}}}^\perp \mathcal{P}_{T_0}\|) \|\mathcal{P}_{T_0} \mathcal{P}_{\Omega_{\mathcal{A}}}^\perp(N_{\mathcal{A}})\|_F^2 \\ &\geq \frac{1}{2} \|\mathcal{P}_{T_0} \mathcal{P}_{\Omega_{\mathcal{A}}}^\perp(N_{\mathcal{A}})\|_F^2, \end{aligned}$$

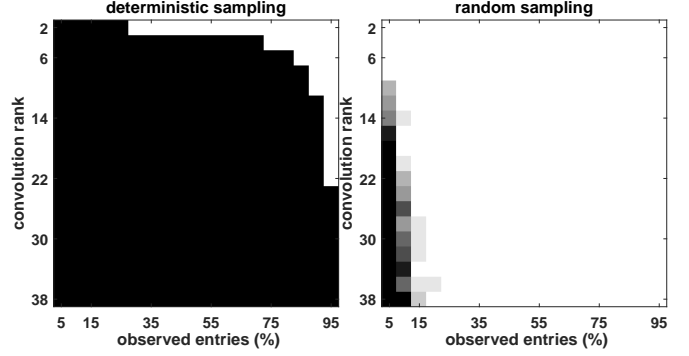


Fig. 6. Investigating the recovery performance of  $\text{DFT}_{\ell_1}$  under the setup of random sampling and forecasting (i.e., deterministic sampling). The white and black areas mean “success” and “failure”, respectively, where the recovery is regarded as being successful iff  $\text{PSNR} > 50$ .

which gives that

$$\begin{aligned} \|\mathcal{P}_{T_0} \mathcal{P}_{\Omega_{\mathcal{A}}}^\perp(N_{\mathcal{A}})\|_F^2 &\leq 2 \|\mathcal{P}_{\Omega_{\mathcal{A}}} \mathcal{P}_{T_0} \mathcal{P}_{\Omega_{\mathcal{A}}}^\perp(N_{\mathcal{A}})\|_F^2 \\ &= 2 \|\mathcal{P}_{\Omega_{\mathcal{A}}} \mathcal{P}_{T_0}^\perp \mathcal{P}_{\Omega_{\mathcal{A}}}^\perp(N_{\mathcal{A}})\|_F^2 \leq 2(38k + 2\sqrt{k})^2 \epsilon^2. \end{aligned}$$

Combining the above justifications, we have

$$\begin{aligned} \|N_{\mathcal{A}}\|_F &\leq \|\mathcal{P}_{T_0} \mathcal{P}_{\Omega_{\mathcal{A}}}^\perp(N_{\mathcal{A}})\|_F + \|\mathcal{P}_{T_0} \mathcal{P}_{\Omega_{\mathcal{A}}}(N_{\mathcal{A}})\|_F \\ &\quad + \|\mathcal{P}_{T_0}^\perp(N_{\mathcal{A}})\|_F \leq (\sqrt{2} + 1)(38k + 2\sqrt{k})\epsilon. \end{aligned}$$

Finally, the fact  $\|N\|_F = \|N_{\mathcal{A}}\|_F / \sqrt{k}$  finishes the proof.  $\square$

## 6 EXPERIMENTS

All experiments are conducted on a workstation equipped with two Intel(R) Xeon(R) E5-2620 v4 2.10GHz CPU processors and 256GB RAM. All the methods considered for comparison are implemented using Matlab 2019a, and the codes are available at <https://github.com/gcliu1982/CNNM>.

### 6.1 Simulations

We shall verify the proved theories by synthetic data. We generate  $M$  and  $L_0$  according to a model as follows:  $[M]_t = [L_0]_t = \sum_{i=1}^a \sin(2ti\pi/m)$ , where  $m = 1000$ ,  $t = 1, \dots, m$  and  $a = 1, \dots, 19$ . So the target  $L_0$  is a univariate time series of dimension 1000, with  $\|\mathcal{F}(L_0)\|_0 = 2a$  and  $\mu_m(L_0) = 1$ . The values in  $L_0$  are further normalized to have a maximum of 1. Regarding the locations of observed entries, we consider two settings: One is to randomly select a subset of entries as in Figure 3(c), referred to as “random sampling”, the other is the forecasting setup used in Figure 3(b), referred to as “deterministic sampling”. The observation fraction is set as  $\rho_0 = 0.05, 0.1, \dots, 0.95$ . For the setup of random sampling, we run 20 trials, and thus there are  $19 \times 19 \times 21 = 7581$  simulations in total.

The results are shown in Figure 6, the left part of which illustrates that the bound proven in Corollary 4.1 is indeed tight. As we can see, the recovery of future observations is much more challenging than restoring the missing entries chosen randomly. In fact, forecasting is exactly the *worst case* of tensor completion. In these experiments, the convolution rank  $r_k(L_0)$  does not grow with the kernel size, so there is no benefit to try different kernel sizes in CNNM.

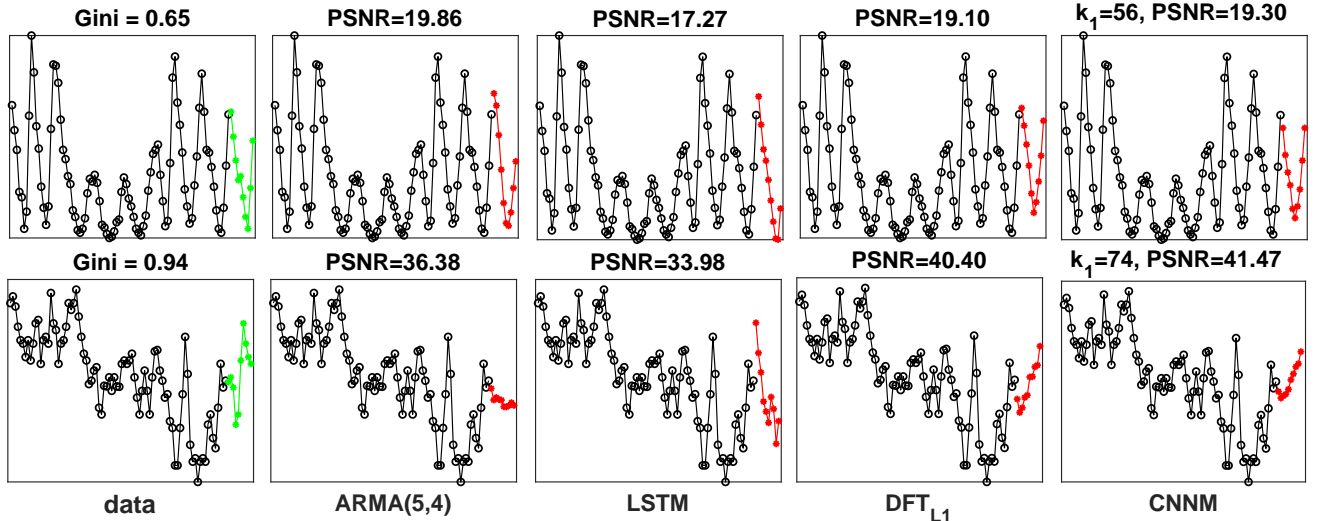


Fig. 7. Results for univariate time series forecasting. The left figure shows the entire series used for experiments, where the observed and future entries are plotted with black and green markers, respectively.

TABLE 1

Comparison results obtained on 10 time series from TSDL, in terms of PSNR and running time.

methods	PSNR				averaged time (secs)
	max	min	mean	std	
ARMA(2,3)	33.84	5.63	20.77	7.26	1.67
LSTM	34.88	13.17	20.38	<b>7.03</b>	46.35
DFT <sub><math>\ell_1</math></sub>	40.40	12.86	21.58	7.89	<b>0.01</b>
CNNM( $k_1 = 0.3m$ )	40.47	<b>14.23</b>	21.92	7.79	1.02
CNNM( $k_1 = 0.4m$ )	40.85	<b>14.23</b>	<b>21.93</b>	7.80	1.77
CNNM( $k_1 = 0.5m$ )	<b>41.15</b>	14.12	21.88	7.83	2.77

## 6.2 Univariate Time Series Forecasting

Now we consider two real-world time series downloaded from Time Series Data Library (TSDL): One for the annual Wolfer sunspot numbers from 1770 to 1869 with  $m = 100$ , and the other for the highest mean monthly levels of Lake Michigan from 1860 to 1955 with  $m = 96$ . We consider for comparison the well-known methods of ARMA and LSTM.<sup>4</sup> ARMA contains many hyper-parameters, which are manually tuned to maximize its recovery accuracy (in terms of PSNR) on the first sequence. The LSTM architecture used for experiment is consist of four layers, including an input layer with 1 unit, a hidden LSTM layer with 200 units, a fully connected layer and a regression layer. The results are shown in Figure 7. Via manually choosing the best parameters, ARMA can achieve the best performance on the first dataset. But its results are unsatisfactory while applying the same parametric setting to the second one. By contrast, DFT <sub>$\ell_1$</sub>  produces reasonable results on both datasets that differ greatly in the evolution rules. This is not incredible, because the method never assumes explicitly how the future entries are related to the previously observed ones, and it is indeed the Fourier sparsity of the series itself that enables the recovery of the unseen future data.

We have in hand 10 univariate time series from TSDL. These sequences have different dimensions ranging from 56 to 1461 and Fourier Gini indices from 0.52 to 0.94. For each sequence, its last 10 percent is treated as the unseen future

4. Unlike the recent proposed deep architectures, the classical LSTM supports the setup of only one sequence.

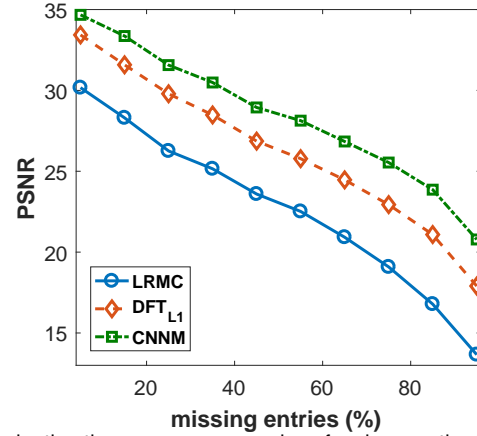


Fig. 8. Evaluating the recovery accuracies of various methods, using the  $200 \times 200$  Lena image as the experimental data. The missing entries are chosen uniformly at random, and the numbers plotted above are averaged from 20 random trials.

data. Since the previously used ARMA(5,4) model needs a considerable number of historical samples to train and occasionally gets crashed while dealing with short sequences, we consider instead an ARMA(2,3) model as the baseline. The comparison results are shown in Table 1. It can be seen that DFT <sub>$\ell_1$</sub>  outperforms ARMA(2,3) and LSTM, in terms of both recovery accuracy and computational efficiency. Via choosing proper kernel sizes, CNNM can future outperform DFT <sub>$\ell_1$</sub> , though the improvements here are not dramatic. While dealing with images and videos, the recovery accuracy of CNNM is distinctly higher than that of DFT <sub>$\ell_1$</sub> , as will be shown in the next two subsections.

## 6.3 Image Completion

The proposed methods, DFT <sub>$\ell_1$</sub>  and CNNM, are indeed general methods for completing sequential tensors rather than specific forecasting models. To validate their completion performance, we consider the task of restoring the  $200 \times 200$  Lena image from its incomplete versions. We also include the results of LRMC [13] for comparison. Figure 8 evaluates the recovery performance of various methods. It is clear that LRMC is distinctly outperformed by DFT <sub>$\ell_1$</sub> , which is



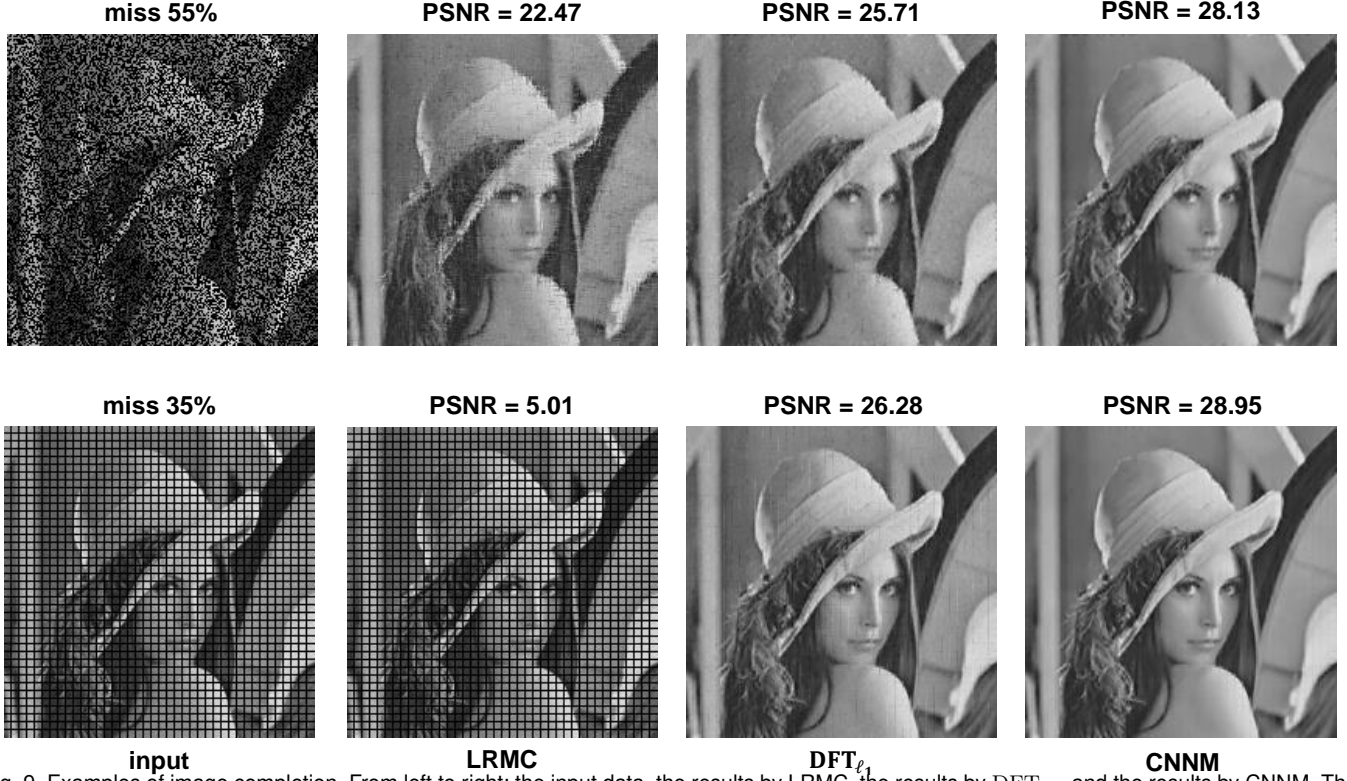


Fig. 9. Examples of image completion. From left to right: the input data, the results by LRMC, the results by  $DFT_{\ell_1}$ , and the results by CNNM. The Gini index of the Fourier transform of the original Lena image is 0.79. Note that the PSNR value is computed only on the missing entries. When evaluating over the whole image, the PSNR of the image at the lower right corner is about 36.

TABLE 2

PSNR and running time on the  $200 \times 200$  Lena image. In these experiments, 60% of the image pixels are randomly chosen to be missing. The numbers shown below are collected from 20 runs.

Methods	PSNR	Time (seconds)
LRMC	$21.65 \pm 0.06$	$18.7 \pm 0.5$
$DFT_{\ell_1}$	$25.13 \pm 0.06$	<b><math>0.51 \pm 0.01</math></b>
CNNM( $13 \times 13$ )	$27.20 \pm 0.11$	$65.3 \pm 0.8$
CNNM( $23 \times 23$ )	$27.45 \pm 0.12$	$257 \pm 3$
CNNM( $33 \times 33$ )	$27.53 \pm 0.12$	$717 \pm 12$
CNNM( $43 \times 43$ )	$27.57 \pm 0.12$	$1478 \pm 24$
CNNM( $53 \times 53$ )	<b><math>27.58 \pm 0.11</math></b>	$2630 \pm 69$
CNNM( $63 \times 63$ )	$27.57 \pm 0.11$	$5482 \pm 96$

further outperformed largely by CNNM. Figure 9 shows that the images restored by CNNM is visually better than  $DFT_{\ell_1}$ , whose results contain many artifacts but are still better than LRMC. In particular, the second row of Figure 9 illustrates that CNNM can well handle the difficult cases where some rows and columns of an image are wholly missing. Table 2 shows some detailed evaluation results. As we can see, when the kernel size rises from  $13 \times 13$  to  $53 \times 53$ , the PSNR produced by CNNM only slightly increases from 27.2 to 27.58. However, since the computational complexity of CNNM is  $O(mk^2)$ , the running time grows fast as the enlargement of the kernel size. So, we would suggest setting  $k_1 = k_2 = 13$  while running CNNM on natural images.

#### 6.4 Video Completion and Prediction

We create a  $50 \times 50 \times 62$  video consisting of a sequence of  $50 \times 50$  images patches quoted from the CDnet 2014 database [63], see Figure 10. We first consider a completion task of restoring the video from some randomly chosen entries. To show the advantages of the proposed



Fig. 10. All 62 frames of the  $50 \times 50 \times 62$  video used for experiments. This sequence records the entire process that a bus passes through a certain location on a highway. The Gini index of the Fourier transform of this dataset is 0.73.

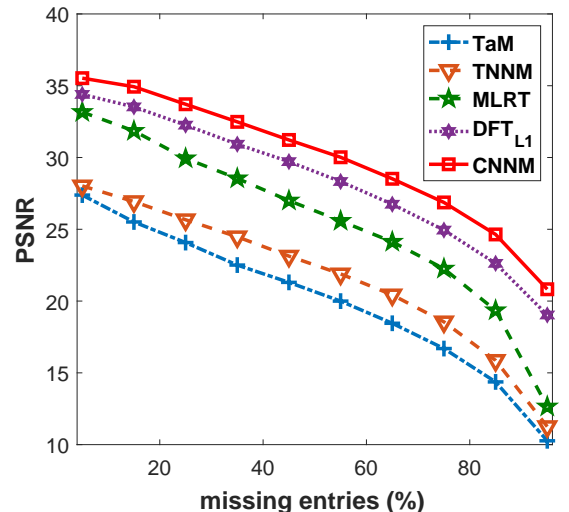


Fig. 11. Evaluation results of restoring the  $50 \times 50 \times 62$  video from randomly selected entries. The numbers plotted above are averaged from 20 random trials.

TABLE 3

Evaluation results (PSNR) of video prediction. The task is to forecast the last 6 frames given the former 56 frames. For CNNM, the first two quantities of the kernel size are fixed as  $k_1 = k_2 = 13$ .

Methods	1st	2st	3st	4st	5st	6st
TaM	5.22	5.49	5.75	5.96	6.15	6.23
TNNM	5.22	5.49	5.75	5.96	6.15	6.23
MLRT	5.22	5.49	5.75	5.96	6.15	6.23
LSTM	20.17	18.80	17.01	16.49	14.73	11.83
DFT $_{\ell_1}$	22.56	19.53	18.72	19.43	21.21	26.20
CNNM( $k_3 = 13$ )	23.48	20.64	20.02	20.80	23.07	28.18
CNNM( $k_3 = 31$ )	24.27	21.65	21.17	22.10	24.49	29.72
CNNM( $k_3 = 62$ )	<b>24.57</b>	<b>22.01</b>	<b>21.56</b>	<b>22.56</b>	<b>24.98</b>	<b>30.32</b>

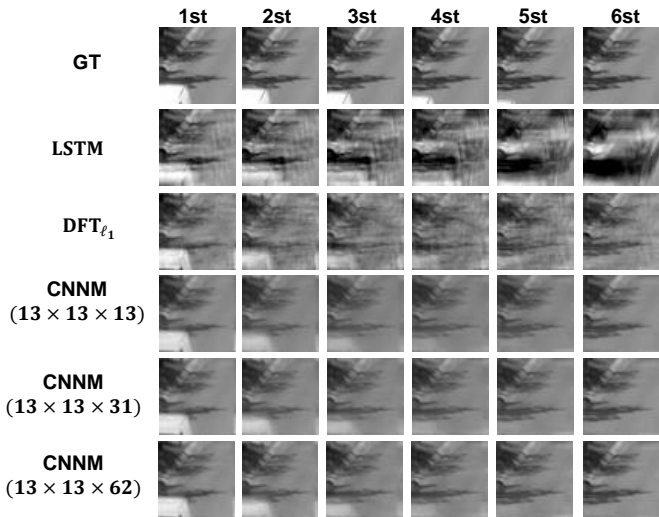


Fig. 12. Visual results of video prediction. The goal of the task is to forecast the last 6 frames given the former 56 frames.

methods, we include for comparison three OTC methods, including Tensor as a Matrix (TaM) [13], Tensor Nuclear Norm Minimization (TNNM) [15] and Mixture of Low-Rank Tensors (MLRT) [17]. As shown in Figure 11, DFT $_{\ell_1}$  dramatically outperforms all OTC methods that ignore the spatio-temporal structures encoded in the video. But DFT $_{\ell_1}$  is further outperformed distinctly by CNNM ( $13 \times 13 \times 13$ ); this confirms the benefits of controlling the kernel size.

We now consider a forecasting task of recovering the last 6 frames from the former 56 frames. Similar to the experimental setup of Section 6.2, the LSTM network used here also contains 4 layers. The number of input units and LSTM hidden units are 2500 and 500, respectively. Since there is only one sequence, the learning problem for training the LSTM network may be severely ill-conditioned. Table 3 validates the effectiveness of various methods. As we can see, OTC methods (including TaM, TNNM and MLRT) produce very poor results. In fact, all these methods predict the future data as zero. The PSNR values achieved by LSTM are very low; this is not strange, because there are no extra training sequences. As shown in Figure 12, DFT $_{\ell_1}$  owns certain ability to forecast the future data, but the obtained images are full of artifacts. By contrast, the quality of the images predicted by CNNM is much higher.

## 7 CONCLUSION AND FUTURE WORK

In this work, we studied a significant problem called *future data recovery*, with the purpose of tackling the identifiability

issue of the unseen future observations. We first reformulated the problem to a special tensor completion task entitled STC, which targets at restoring a certain amount of missing entries selected—in an arbitrary fashion—from some target tensor  $L_0$  that is supposed to be sequential and not permutable. We then showed that the STC problem, under certain situations, can be well solved by the classical DFT $_{\ell_1}$  method and its generalization called CNNM. Namely, we proved that, whenever the target  $L_0$  is low-rank in some convolution domain, DFT $_{\ell_1}$  and CNNM strictly succeed in recovering  $L_0$ . Even if the prior expectation is not met exactly, they still ensure the success of recovery to some extent. Finally, experiments on some realistic datasets suggested that DFT $_{\ell_1}$  and CNNM are promising methods for data forecasting.

While effective, as aforementioned, CNNM contributes only to a certain case of the STC problem, namely the data tensor should own similar structures to natural images or videos such that its convolution matrix is low-rank or approximately so. There are many other sequential tensors cannot be handled by CNNM, for which the idea of *graph convolution* [64] might be promising. Moreover, with the help of *learning-based optimization* [58, 59], it is possible to generalize CNNM to some learnable deep architecture. But we would leave these as future work.

## ACKNOWLEDGEMENT

This work is supported in part by New Generation AI Major Project of Ministry of Science and Technology of China under Grant 2018AAA0102501, in part by SenseTime Research Fund.

## REFERENCES

- [1] C. Chatfield, *Time-Series Forecasting*. New York, USA: Chapman and Hall/CRC, 2000.
- [2] J. G. Gooijera and R. J. Hyndmanb, “25 years of time series forecasting,” *International Journal of Forecasting*, vol. 22, no. 3, pp. 443–473, 2006.
- [3] N. I. Sapankevych and R. Sankar, “Time series prediction using support vector machines: A survey,” *IEEE Computational Intelligence Magazine*, vol. 4, no. 2, pp. 24–38, 2009.
- [4] G. P. Zhang, “Time series forecasting using a hybrid arima and neural network model,” *Neurocomputing*, vol. 50, pp. 159–175, 2003.
- [5] M. Mathieu, C. Couprie, and Y. LeCun, “Deep multi-scale video prediction beyond mean square error,” in *International Conference on Learning Representations*, 2016, pp. 1–14.
- [6] J. Brownlee, *Deep Learning for Time Series Forecasting*. Ebook, 2018.
- [7] S. Hochreiter and J. Schmidhuber, “Long short-term memory,” *Neural Computation*, vol. 9, no. 8, pp. 1735–1780, 1997.
- [8] X. Shi, Z. Chen, H. Wang, D.-Y. Yeung, W.-k. Wong, and W.-c. Woo, “Convolutional LSTM network: A machine learning approach for precipitation nowcasting,” in *Advances in Neural Information Processing Systems*. Curran Associates, Inc., 2015, pp. 802–810.



- [9] N. Srivastava, E. Mansimov, and R. Salakhutdinov, "Unsupervised learning of video representations using LSTMs," in *International Conference on Machine Learning*, 2015, p. 843C852.
- [10] Y. Wang, Z. Gao, M. Long, J. Wang, and P. S. Yu, "PredRNN++: Towards A resolution of the deep-in-time dilemma in spatiotemporal predictive learning," in *International Conference on Machine Learning*, 2018, pp. 5123–5132.
- [11] S.-F. Wu, C.-Y. Chang, and S.-J. Lee, "Time series forecasting with missing values," in *International Conference on Industrial Networks and Intelligent Systems*, 2015, pp. 151–156.
- [12] Z. Che, S. Purushotham, K. Cho, D. Sontag, and Y. Liu, "Recurrent neural networks for multivariate time series with missing values," *Scientific Reports*, vol. 8, no. 1, pp. 85–98, 2018.
- [13] E. Candès and B. Recht, "Exact matrix completion via convex optimization," *Foundations of Computational Mathematics*, vol. 9, no. 6, pp. 717–772, 2009.
- [14] D. Kressner, M. Steinlechner, and B. Vandereycken, "Low-rank tensor completion by riemannian optimization," *BIT Numerical Mathematics*, vol. 54, no. 2, pp. 447–468, Jun 2014.
- [15] J. Liu, P. Musialski, P. Wonka, and J. Ye, "Tensor completion for estimating missing values in visual data," *IEEE Transactions on Pattern Analysis and Machine Intelligence*, vol. 35, no. 1, pp. 208–220, Jan 2013.
- [16] M. Signoretto, R. V. de Plas, B. D. Moor, and J. A. Suykens, "Tensor versus matrix completion: A comparison with application to spectral data," *IEEE Signal Processing Letters*, vol. 18, no. 7, pp. 403–406, 2011.
- [17] R. Tomioka, K. Hayashi, and H. Kashima, "Estimation of low-rank tensors via convex optimization," *Arxiv*, vol. 1, no. 1, pp. 1–19, 2010.
- [18] M. Yuan and C.-H. Zhang, "On tensor completion via nuclear norm minimization," *Foundations of Computational Mathematics*, vol. 16, pp. 1031–1068, 2016.
- [19] P. Zhou, C. Lu, Z. Lin, and C. Zhang, "Tensor factorization for low-rank tensor completion," *IEEE Transactions on Image Processing*, vol. 27, no. 3, pp. 1152–1163, March 2018.
- [20] D. Gross, "Recovering low-rank matrices from few coefficients in any basis," *IEEE Transactions on Information Theory*, vol. 57, no. 3, pp. 1548–1566, 2011.
- [21] H.-F. Yu, N. Rao, and I. S. Dhillon, "Temporal regularized matrix factorization for high-dimensional time series prediction," in *Advances in Neural Information Processing Systems* 28, 2016, pp. 847–855.
- [22] J. Yoon, J. Jordon, and M. van der Schaar, "GAIN: Missing data imputation using generative adversarial nets," in *International Conference on Machine Learning*, 2018, pp. 5689–5698.
- [23] C. Lu, J. Feng, Y. Chen, W. Liu, Z. Lin, and S. Yan, "Tensor robust principal component analysis with a new tensor nuclear norm," *IEEE Transactions on Pattern Analysis and Machine Intelligence*, vol. 1, no. 1, pp. 1–14, 2019.
- [24] A. Chandrakasan, V. Gutnik, and T. Xanthopoulos, "Data driven signal processing: an approach for energy efficient computing," in *International Symposium on Low Power Electronics and Design*, 1996, pp. 347–352.
- [25] I. Daubechies, O. Runborg, and J. Zou, "A sparse spectral method for homogenization multiscale problems," *Multiscale Modeling & Simulation*, vol. 6, no. 3, pp. 711–740, 2007.
- [26] D. Donoho, "Compressed sensing," *IEEE Transactions on Information Theory*, vol. 52, no. 4, pp. 1289–1306, 2006.
- [27] H. Hassanieh, P. Indyk, D. Katabi, and E. Price, "Simple and practical algorithm for sparse fourier transform," in *Twenty-third Annual ACM-SIAM Symposium on Discrete Algorithms*, 2012, pp. 1183–1194.
- [28] E. Kushilevitz and Y. Mansour, "Learning decision trees using the fourier spectrum," in *Annual ACM Symposium on Theory of Computing*, 1991, pp. 455–464.
- [29] A. P. V. Mengda Lin, "A low complexity high resolution cooperative spectrum-sensing scheme for cognitive radios," *Circuits, Systems, and Signal Processing*, vol. 31, no. 3, pp. 1127–1145, 2012.
- [30] R. O'Donnell, "Some topics in analysis of boolean functions," in *Annual ACM Symposium on Theory of Computing*, 2008, pp. 569–578.
- [31] E. Candès, J. Romberg, and T. Tao, "Robust uncertainty principles: exact signal reconstruction from highly incomplete frequency information," *IEEE Transactions on Information Theory*, vol. 52, no. 2, pp. 489–509, 2006.
- [32] E. Candès and M. Wakin, "An introduction to compressive sampling," *IEEE Signal Processing Magazine*, vol. 25, no. 2, pp. 21–30, 2008.
- [33] D. Gabay and B. Mercier, "A dual algorithm for the solution of nonlinear variational problems via finite element approximation," *Computers and Mathematics with Applications*, vol. 2, no. 1, pp. 17–40, 1976.
- [34] Z. Lin, M. Chen, and Y. Ma, "The augmented lagrange multiplier method for exact recovery of corrupted low-rank matrices," *UIUC Technical Report UILU-ENG-09-2215*, 2009.
- [35] G. Liu, S. Chang, and Y. Ma, "Blind image deblurring using spectral properties of convolution operators," *IEEE Transactions on Image Processing*, vol. 23, no. 12, pp. 5047–5056, 2014.
- [36] E. Candès and T. Tao, "Decoding by linear programming," *IEEE Transactions on Information Theory*, vol. 51, no. 12, pp. 4203–4215, 2005.
- [37] M. Fazel, "Matrix rank minimization with applications," *PhD thesis*, 2002.
- [38] B. Recht, M. Fazel, and P. Parrilo, "Guaranteed minimum-rank solutions of linear matrix equations via nuclear norm minimization," *SIAM Review*, vol. 52, no. 3, pp. 471–501, 2010.
- [39] L. D. Lathauwer, B. D. Moor, and J. Vandewalle, "A multilinear singular value decomposition," *SIAM Journal on Matrix Analysis and Applications*, vol. 21, no. 4, pp. 1253–1278, 2000.
- [40] M. F. Fahmy, G. M. A. Raheem, U. S. Mohamed, and O. F. Fahmy, "A new fast iterative blind deconvolution algorithm," *Journal of Signal and Information Processing*, vol. 3, no. 1, pp. 98–108, 2012.
- [41] M. K. Ng, R. H. Chan, and W.-C. Tang, "A fast algorithm for deblurring models with neumann boundary conditions," *SIAM J. Sci. Comput.*, vol. 21, no. 3, pp. 851–866, 1999.

- [42] Y. Wang, J. Yang, W. yin, and Y. Zhang, "A new alternating minimization algorithm for total variation image reconstruction," *SIAM Journal on Imaging Sciences*, vol. 1, no. 3, pp. 248–272, 2008.
- [43] M. Combesure, "Block-circulant matrices with circulant blocks, weil sums, and mutually unbiased bases. ii. the prime power case," *Journal of Mathematical Physics*, vol. 50, no. 3, pp. 1–14, 2009.
- [44] J. Cai, E. Candes, and Z. Shen, "A singular value thresholding algorithm for matrix completion," *SIAM J. on Optimization*, vol. 20, no. 4, pp. 1956–1982, 2010.
- [45] C. Fang, F. Cheng, and Z. Lin, "Faster and non-ergodic  $o(1/k)$  stochastic alternating direction method of multipliers," in *Advances in Neural Information Processing Systems*, 2017, pp. 4476–4485.
- [46] G. Liu, Z. Lin, S. Yan, J. Sun, Y. Yu, and Y. Ma, "Robust recovery of subspace structures by low-rank representation," *IEEE Transactions on Pattern Recognition and Machine Intelligence*, vol. 35, no. 1, pp. 171–184, 2013.
- [47] M. Frigo and S. G. Johnson, "Fftw: an adaptive software architecture for the fft," in *International Conference on Acoustics, Speech and Signal Processing*, vol. 3, 1998.
- [48] G. Liu, Q. Liu, and X.-T. Yuan, "A new theory for matrix completion," in *Neural Information Processing Systems*, 2017, pp. 785–794.
- [49] G. Liu, Q. Liu, X.-T. Yuan, and M. Wang, "Matrix completion with deterministic sampling: Theories and methods," *IEEE Transactions on Pattern Analysis and Machine Intelligence*, vol. 1, no. 1, pp. 1–18, 2019.
- [50] X. Liang, X. Ren, Z. Zhang, and Y. Ma, "Repairing sparse low-rank texture," in *European Conference on Computer Vision*, 2012, pp. 482–495.
- [51] G. Liu and P. Li, "Low-rank matrix completion in the presence of high coherence," *IEEE Transactions on Signal Processing*, vol. 64, no. 21, pp. 5623–5633, 2016.
- [52] T. Zhao, Z. Wang, and H. Liu, "A nonconvex optimization framework for low rank matrix estimation," in *Neural Information Processing Systems*, 2015, pp. 559–567.
- [53] R. Ge, J. D. Lee, and T. Ma, "Matrix completion has no spurious local minimum," in *Neural Information Processing Systems*, 2016, pp. 2973–2981.
- [54] R. Sun and Z.-Q. Luo, "Guaranteed matrix completion via non-convex factorization," *IEEE Transactions on Information Theory*, vol. 62, no. 11, pp. 6535 – 6579, 2016.
- [55] Y. Chen, "Incoherence-optimal matrix completion," *IEEE Transactions on Information Theory*, vol. 61, no. 5, pp. 2909–2923, 2015.
- [56] Y. Ma, H. Derksen, W. Hong, and J. Wright, "Segmentation of multivariate mixed data via lossy data coding and compression," *IEEE Transactions on Pattern Analysis and Machine Intelligence*, vol. 29, no. 9, pp. 1546–1562, 2007.
- [57] N. Hurley and S. Rickard, "Comparing measures of sparsity," *IEEE Transactions on Information Theory*, vol. 55, no. 10, pp. 4723–4741, 2009.
- [58] K. Gregor and Y. LeCun, "Learning fast approximations of sparse coding," in *International Conference on International Conference on Machine Learning*, 2010, pp. 399–406.
- [59] X. Xie, J. Wu, Z. Zhong, G. Liu, and Z. Lin, "Differentiable linearized ADMM," in *International Conference on Machine Learning*, vol. 97, 2019, pp. 6902–6911.
- [60] I. Daubechies, M. Defrise, and C. D. Mol, "An iterative thresholding algorithm for linear inverse problems with a sparsity constraint," *Communications on Pure and Applied Mathematics*, vol. 57, no. 11, pp. 1413–1457, 2004.
- [61] L. Yann, B. Boser, J. S. Denker, D. Henderson, R. E. Howard, W. Hubbard, and L. D. Jackel, "Handwritten digit recognition with a back-propagation network," in *Advances in Neural Information Processing Systems*, 1990, pp. 396–404.
- [62] R. T. Rockafellar, *Convex Analysis*. Princeton, NJ, USA: Princeton University Press, 1970.
- [63] Y. Wang, P.-M. Jodoin, F. Porikli, J. Konrad, Y. Benezeth, and P. Ishwar, "Cdnets 2014: An expanded change detection benchmark dataset," in *IEEE Conference on Computer Vision and Pattern Recognition Workshops*, 2014, pp. 393–400.
- [64] J. Bruna, W. Zaremba, A. Szlam, and Y. LeCun, "Spectral networks and locally connected networks on graphs," in *International Conference on Learning Representations*, 2014, pp. 1–14.